Organometallic interactions between metal nanoparticles and carbon-based molecules: A surface reactivity rationale

Ekaterina Mamontova, Isabelle Favier, Daniel Pla, Montserrat Gómez

Organometallic interactions between metal nanoparticles and carbon-based molecules: a surface reactivity rationale

Ekaterina Mamontova, Isabelle Favier, Daniel Pla and Montserrat Gómez*
Laboratoire Hétérochimie Fondamentale et Appliquée, CNRS UMR 5069, Université Toulouse 3 – Paul Sabatier, 118 route de Narbonne, 31062 Toulouse Cedex 09, France
*Corresponding author: e-mail address: gomez@chimie.ups-tlse.fr

ORCID
Ekaterina Mamontova https://orcid.org/0000-0002-4959-3332
Isabelle Favier https://orcid.org/0000-0002-0590-0708
Daniel Pla https://orcid.org/0000-0002-8703-8778
Montserrat Gómez https://orcid.org/0000-0003-1211-1333

Keywords: Metal-based nanoparticles, C-C couplings, C-heteroatom couplings, Mechanistic insights, Surface reactivity

ABSTRACT Metal-based nanoparticles (MNPs) have been widely used as catalysts in different types of chemical transformations, taking advantage of their intrinsic properties, such as geometry, specific surface area, sites (edges, corners, faces, kinks, steps…) and electronic configuration, which offer a wide-ranging variety of interactions with the reagents and products of catalytic processes. In addition, both the nature of the metal and the support (often MNPs are supported on solids or immobilized in liquid phases) play a crucial role in their catalytic behavior and plausible recycling. Nevertheless, research works reporting on the organometallic interactions at the metal surface are much more limited, often due to the difficulty of accessing to convenient experimental techniques. In this contribution, an overview from an organometallic point of view is presented regarding the interactions of organic compounds (reactants or products) at the surface of metal nanoparticles based on experimental data and calculations, helping to establish structure-reactivity correlations.

Contents

1. INTRODUCTION

Distinct metal-based nanoparticles, with dimensions in the range of 1–100 nm, have tackled a huge development over the last decades, due to their unique physical and chemical properties compared to extended materials (e.g. coordination polymers or bulk metals) or molecular-based compounds. Actually, this exclusive behavior is essentially due to structural and electronic outcomes of nanomaterials, in particular allowing widespread sorts of catalytic transformations.[1-5] Although metal nanoparticles have been largely employed in heterogeneous catalysis, specifically with significant contributions regarding the oil sector,[6] nanocatalysis emerged at the end of 1990s allowing control and fine-tuning of morphology and surface state of the as-prepared nano-objects. The advances in full characterization of nanomaterials using innovative techniques, provide a rational design of catalysts at nanometric scale.[7-10] Undoubtedly, reproducible synthetic methods affording MNPs with a tight control of structure and composition are conclusive for their applications.

MNPs are commonly prepared by chemical (bottom-up) or physical (top-down) approaches.[11,12] Chemical methods are generally classified in colloidal synthesis, including different activation modes (conventional heating, ultrasounds, microwaves, photolysis, electrochemistry…),[12-14] and chemical vapor deposition.[15-18] Top-down procedures consist in the transformation of bulk materials into nano-structures by different ways (lase ablation, thermal activation, mechanical milling);[19-22] in particular, sputtering deposition of metal atoms or small clusters on a solid or a liquid phase seems an appropriate methodology to prepare well-defined nano-materials.[11,23-25]

The applications of metal-based nanoparticles, including polymetallic materials, take account of a large panel of transformations. In the frame of Fine Chemistry (pharmaceuticals compounds, agrochemicals, natural products…), metal-catalyzed coupling reactions occupy a privileged position for their versatility (C-C and C-heteroatom bond formation processes, including tandem and sequential transformations).[26-28] These types of reactions are often multi-parameters, involving various reagents other than substrates, such as bases. Under these “cocktail” conditions, metal lixiviation from the MNP surface can occur, and thus MNPs act as reservoir of catalytically active species.[29-31] However, deep mechanistic studies have permitted to identify surface-like reactivity for different C-C or C-heteroatom couplings, exhibiting fine-tuning between the adsorption of reagents and products, permitting selective reactivity and avoiding catalyst poisoning.

This review focuses on the reported works concerning C-C and C-heteroatom couplings catalyzed by MNPs, providing a special insight on metal surface-organic compounds interactions, based on experimental data including theoretical calculations, material characterization and control tests.

2. C-C HOMO-COUPLING REACTIONS

C-C bond formation transformations through metal-catalyzed homo-coupling reactions represent a useful and sustainable tool in organic synthesis. In this section, C(sp^2)-C(sp^2) (Ullmann-type reactions catalyzed by Cu-, Co-, Pd- and Au-based nanoparticles) and C(sp)-C(sp) (Glaser couplings with metal-based nanoparticles from group 11) homo-couplings are reviewed, reporting mechanistic approaches in order to elucidate the role of the metal surface in the corresponding coupling. The multi-component Guerbet reaction is also discussed.

2.1. Ullmann and boronic acid couplings

Symmetrical biaryl compounds are involved in a wide range of applications (rigid liquid crystals, drugs, polymers, ligands for organometallic complexes…). Many synthetic methodologies have been reported in the literature, including metal-catalyzed homocoupling approaches where palladium is mostly used but also other transition metals (copper, gold, iron…) have been efficiently applied.[32] In this frame, different reagents are used, such as aryl halides, boronic acids, arenediazonium salts and aryl organometallic compounds, among the commonest ones.

One of the oldest metal-catalyzed reactions for making C-C bonds between aryl groups is the classical Cu-mediated Ullmann coupling, using aryl halides as reagents. Since the earliest works reported by Ullmann and Goldberg also including the formation of amides and ethers,[33,34] a myriad of methodologies with different transition metal catalysts has been developed to form C(sp^2)-C(sp^2) and

Csp^2-heteroatom bonds. These ways overcome the main limitations of the classical Ullmann coupling and in consequence permit to work under milder conditions, using inactivated substrates and exhibiting a better tolerance to functional groups.[35-39]

Sykes' group has studied the Ullmann coupling of bromobenzene on a Cu(111) surface by Scanning Tunnelling Microscopy (STM).[40] They demonstrated that the formation of biphenyl occurs at the metal surface through a mobile organometallic intermediate, containing two phenyl groups bound to a Cu atom that was extracted from the surface (Fig. 1). They could also conclude that the formation of this molecular intermediate at low temperature (160 K) is consistent with the rate limiting step for the studied reaction, being the biphenyl formation and not the Cu atom extraction from the metal surface or the formation of the organometallic intermediate, the step showing the highest energy barrier.

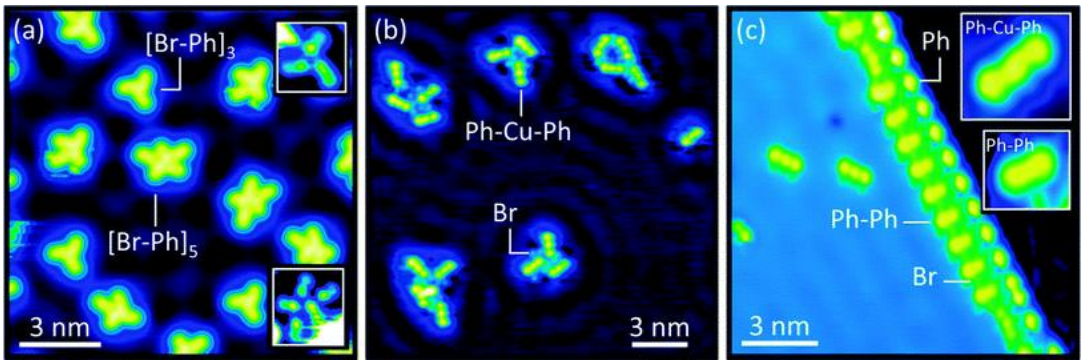

Fig. 1 STEM images showing the progression of the Ullmann coupling on Cu(111) (imaging at 5K): a) Bromobenzene on Cu(111) annealed to 80 K; insets corresponding to high-resolution images of the clusters (3 and 5 molecules); b) clusters of the Ullmann organometallic intermediates and bromo atoms at the copper surface after annealing at 160 K; c) formation of biphenyl after annealing at 350 K; insets corresponding to high-resolution images of the organometallic Ph-Cu-Ph intermediate and biphenyl product. Reproduced from [40] with permission from the Royal Society of Chemistry.

The same group was also interested in the use of CoNPs grown on a Cu(111) surface for the homocoupling of bromobenzene, proving that Co and Cu catalyze the C-C coupling by different pathways.[41] Thus, authors proved that the *in situ* formed intermediates presented a different structure in relation to those coming from copper. STEM analyses (Scanning Transmission Electron Microscopy) evidenced that the bromobenzene dissociation at CoNPs surface happens at lower temperature (< 80 K) than that observed for Cu(111) surface (160 K). Furthermore, the phenyl groups are linked to the cobalt surface, without forming molecular organometallic species, what means that no cobalt atoms were removed from the nanoparticle surface in contrast to the copper reactivity (Fig. 2). After annealing the sample at 160 K, the formation of biphenyl was complete (for Cu(111), the temperature required was 350 K). Similar behavior was observed using benzylbromide as substrate.

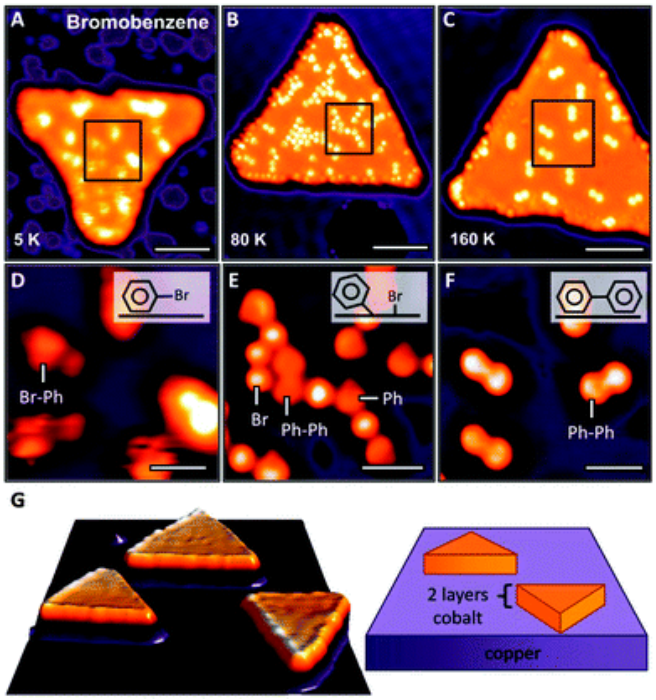

Fig. 2 STEM images displaying the bromobenzene homo-coupling on cobalt nanoparticles: A and D images corresponds to bromobenzene deposited on the Co@Cu(111) surface; B and E images after annealing at 80 K (bromobenzene dissociates in bromo and phenyl species; C and F images corresponds to biphenyl formationon CoNPs (after annealing at 160 K); G shows a schematic representation of the Co/Cu(111) material: cobalt forms triangular nanoparticles on copper. Reproduced from [41] with permission from the Royal Society of Chemistry.

In the last decade, Au- and Pd-based nanoparticles have been efficiently applied to the aryl halide coupling taking advantage of their surface-like reactivity, tolerating both homogeneous (nanoparticles dispersed in a liquid phase) and heterogeneous (nanoparticles immobilized on solids) reaction conditions.[42] Concerning AuNPs supported on semi-conductor materials, Scaiano and coworkers proved the efficiency of AuNPs@TiO_2 in the photoinduced C-C coupling of benzyl derivatives.[43] Control tests demonstrated that the reaction happens through a radical mechanism (radical intermediate trapped by TEMPO) rather than by a nucleophilic substitution reaction, requiring light (530 nm LED), a semi-conductor support and a sacrificial electron donor such as diisopropylethylamine; Au-free TiO_2 gave low yield of the corresponding dimerization product (Fig. 3). Light-promoted coupling of aryl halides was carried out using AuNPs supported on the KNb_3O_8 semi-conductor which exhibits a bigger gap energy between valence and conduction bands than TiO_2 (3.7 eV for KNb_3O_8 vs 3.0 eV for TiO_2), showing a similar mechanism than that described by Scaiano's group.[44]

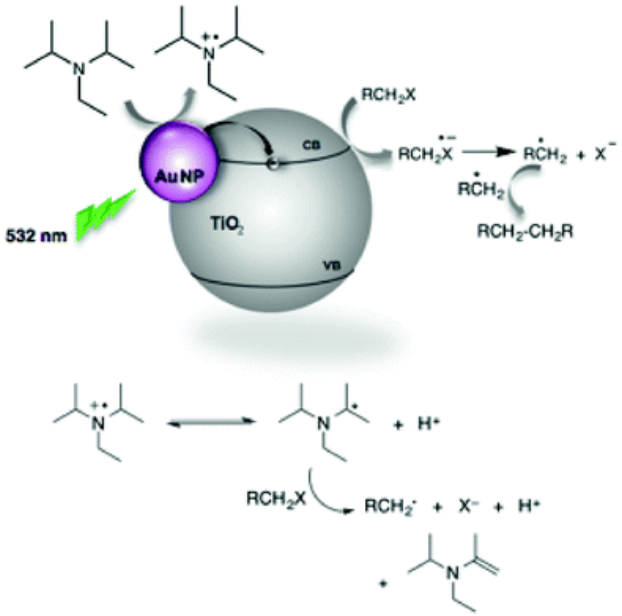

Fig. 3 Top: Plausible mechanism for the AuNPs@TiO_2 catalyzed photocatalytic reductive dimerization of 4-nitrobenzylbromide. Bottom: Reduction of halo-benzyl derivatives by α-aminoalkyl radical intermediates. Reproduced from [43] with permission from the Royal Society of Chemistry.

PdNPs on oxide-based supports have been efficient for aryl halide homo-couplings, some of them proving the synergic effect between the metal surface and the support. Thus, PdNPs immobilized on CeO_2 porous nanorods, which show a large surface area, a considerable concentration of oxygen vacancies and a remarkable basicity, allowed the coupling of chlorobenzene, more difficult to be activated than bromo- and iodo-arenes, in water using glucose as reducing agent.[45] XPS (X-ray Photelectron Spectroscopy) and FT-IR (Fourier Transform Infrared spectroscopy) analyses evidenced that the strong basicity of the support with the high concentration of vacancies, induced a high electron density of surface palladium atoms and in consequence favored the oxidative addition of chloro-arenes at the metal surface, without studying the plausible leaching after this elementary step. Somsook and co-workers studied the synergy between Fe-doped La_2O_3 and PdNPs for a large scope of chloro-arenes, in ethanol under basic conditions.[46] An enhancement of the reactivity was observed using Fe-doped support in comparison to pristine La_2O_3. Based on the materials characterization and catalytic behavior, authors could prove that ethanol (acting also as reducing agent) was activated by La_2O_3 and chloro-arenes by the Pd surface, both processes showing a similar rate (Fig. 4).

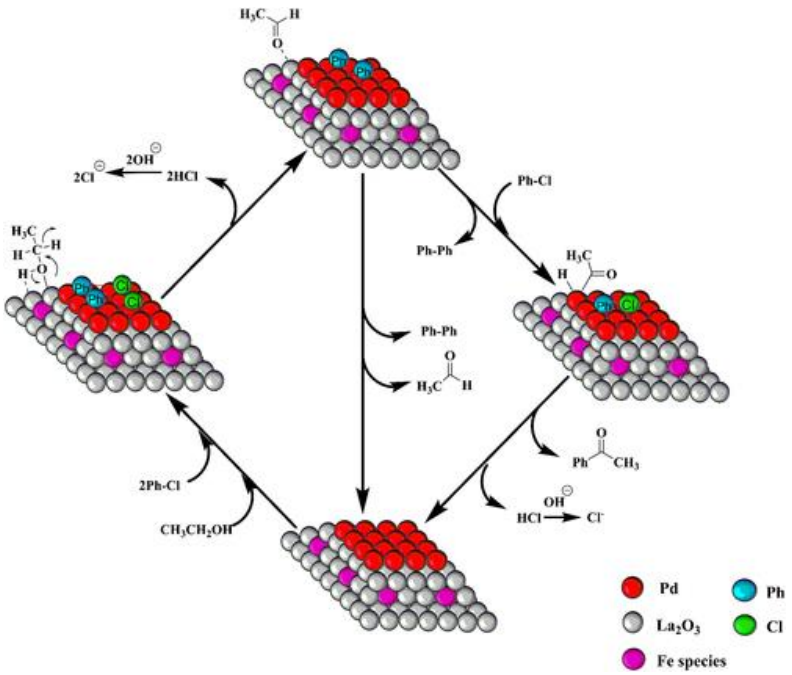

Fig. 4 Plausible mechanism of the formation of aryl methyl ketone and biphenyl catalyzed by PdNPs@Fe-doped La_2O_3. Reproduced from [46] with permission of John Wiley and Sons and Copyright Clearance Center (license number: 5147050704036) 2018.

For PdNPs immobilized on amino-functionalized montmorillonite applied in the Ullmann coupling of iodobenzene, a palladium "release and catch" mechanism was inferred by TEM after several runs (observation of agglomerates), hot filtration test and ICP analyses (leaching of *ca*. 7% of the starting palladium loading).[47]

Hybrid materials constituted by Au-Pd bimetallic nanoparticles (BMNPs) supported on alumina, in the presence of TiO_2 acting as photocatalyst, were applied in Ullmann coupling of aryl halides.[48] XANES analysis of the AuPd BMNPs@Al_2O_3 revealed that both metal atoms are intimately close and an electron density transfer from Pd to Au atoms occurs.[49] The formation of the by-product, benzene, increased linearly with the light intensity, while the formation of biphenyl was constant at high intensities, excluding a radical coupling mechanism. Monitoring and control studies permitted to conclude that the formation of biphenyl is initiated by the photo-generation of phenyl radicals which reacts with an iodobenezene molecule which has been activated at the metal surface (probably promoted by a plasmonic effect); thus, the homo-coupling follows a radical addition-elimination mechanism (Fig. 5).[48]

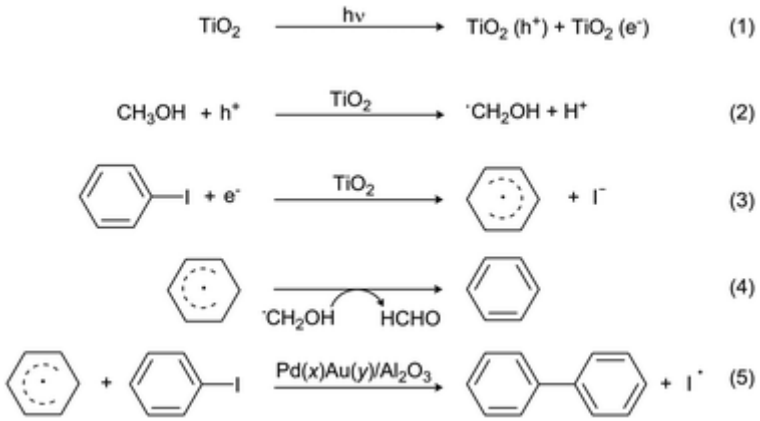

Fig. 5 Plausible mechanism for the photocatalytic homo-coupling of iodobenzene using TiO_2 blended with Au-Pd bimetallic nanoparticles supported on alumina. Reproduced from [48] with permission from the Royal Society of Chemistry.

PdNPs stabilized by polyvinylpyrrolodine (PVP) were efficiently immobilized in glycerol and applied in homocoupling reactions of aryl halides.[50] A deep mechanistic study, including reaction monitoring, electron paramagnetic resonance analyses, effect of radical scavengers and theoretical calculations, permitted to conclude that the reaction occurs through radical intermediates, requiring the synergy between neighboring palladium atoms which lead to the homocoupling product in a regioselective way (Fig. 6).[50]

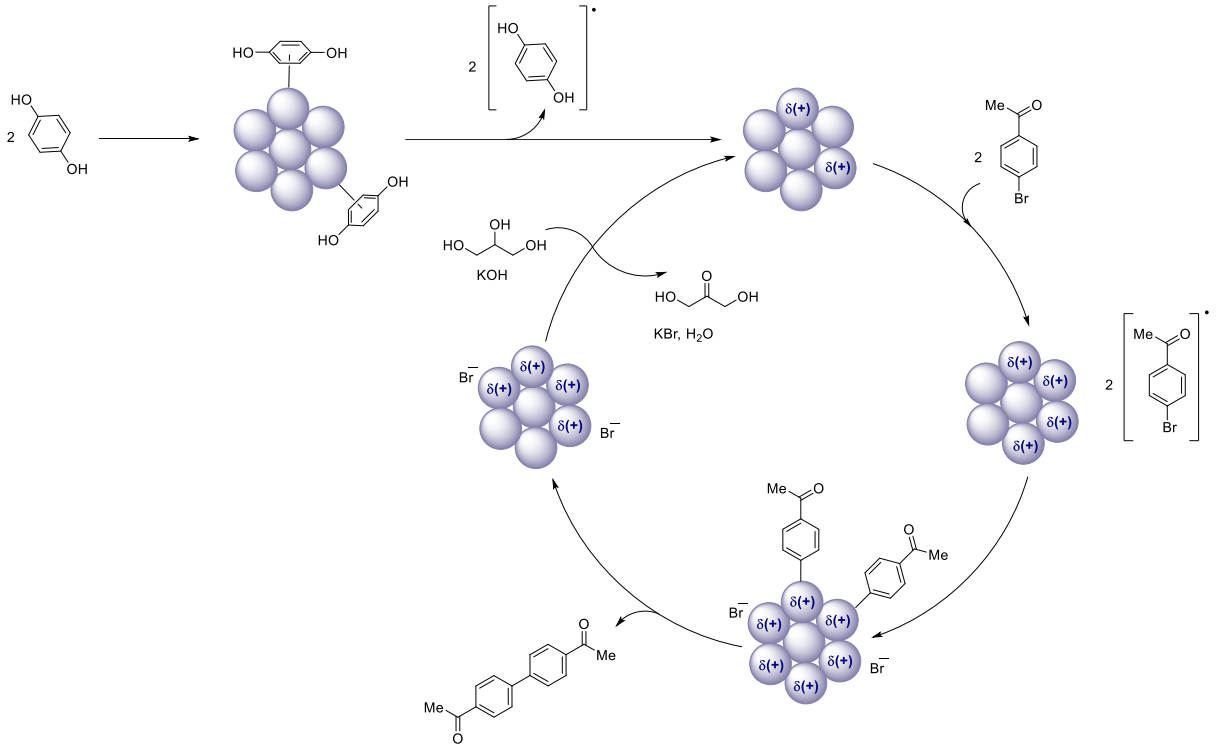

Fig. 6 Proposed mechanism for PdNPs-catalyzed reductive homo-coupling of aryl halide derivatives. Adapted from [50] with permission from the Royal Society of Chemistry.

From a mechanistic point of view, the oxidative coupling of organoboron compounds has aroused great interest in the scientific community, mainly for Pd- and Au-catalyzed processes, using both homogeneous organometallic complexes and well-defined nanoparticles.[51-54] In this latter case, experimental and theoretical studies have been deeply carried out especially with AuNPs.

Corma and co-workers published the first report encompassing Au(III)-based supported ceria heterogeneous catalysts for preparing biaryl compounds through boronic acid homocoupling.[55] In contrast to previous reports, the homocoupling takes place in the absence of both air and added base but requiring the presence of water, which generates hydroxyl groups on CeO_2 surface, responsible of the formation of boric acid. These conditions are probably related to the small gold clusters formed. The formation of H_2 was evidenced by Raman spectroscopy. XPS analyses and IR spectra using CO as a probe molecule, permitted to conclude on the presence of Ce(III) and the correlation between Au(III) and catalytic activity (no correlation found when using Au(I) or Au(0) catalytic materials), proving that Au(III) sites are the active centers.

It is important to highlight that for colloidal AuNPs stabilized by PVP (*ca*. 2 nm), molecular oxygen dissolved in water was found to be necessary to carry out the phenylboronic acid homocoupling.[56] In this context, the O_2 activation necessarily occurs at the metal surface. Based on the theoretical studies performed by Metiu and coworkers,[57] O_2 preferentially binds to coordinative unsaturated Au atoms placed on corners, edges, steps or kinks, but not on faces.

Later on, Corma's group studied the mechanism of activation of $ArB(OH)_2$ considering Au_{38} nanoparticles (AuNPs *ca*. 1 nm) by DFT (Density Functional Theory) calculations,[58] taking into account

that the activation of small molecules is not observed for AuNPs exhibiting diameters larger than *ca*. 4 nm.[59,60] Curiously, it was observed that when the AuNPs are partially oxidized (containing 2 oxygen atoms per Au_{38} NP), the energy barrier associated to the coupling of two aryl groups was lower in energy than in the non-oxidized Au_{38} NP (34.3 kcal/mol *vs* 4.7 kcal/mol). This DFT study proved that the crucial role of O_2 in the homocoupling reaction is related to the coupling step and not to the activation of phenylboronic acid.[58]

2.2. Glaser coupling

The interest for the chemistry of 1,3-diynes has significantly grown in the last years mainly due to their involvement as building blocks in the synthesis of different relevant compounds,[61] such as polymers,[62] natural products,[63] and optoelectronic materials.[64] Usually, 1,3-diynes are obtained by Glaser oxidative coupling, involving both Cu(I)[65] and Cu(II) salts[66] in the presence of ammonia or diamines such as tetramethylethylenediamine, under oxygen atmosphere.[67] In addition to homogeneous catalysts, heterogeneous catalytic materials have been also reported mainly concerning copper and palladium,[68] but also catalytic materials based on other transition metals such as Ni,[69] Ag, and Au.[70,71]

From a mechanistic point of view, it seems difficult that the simultaneous activation of the terminal alkyne and O_2 can take place on isolated copper cations. It is known that Cu-containing enzymes, binuclear metal structures are proposed to be the active sites for O_2 activation;[72] also, in Cu-catalyzed azide-alkyne cycloadditions, it has been demonstrated the role of the multi-nuclear complexes and nanoparticles.[73,74]

Corma and coworkers reported the synthesis of symmetric and unsymmetric 1,3-diynes by oxidative coupling of alkynes catalyzed by CuO_x nanoparticles, both unsupported and supported on nano-TiO_2.[75] This work proved that small Cu-based nanoparticles are necessary (mean diameter *ca*. 2 nm), for both supported and monodispersed CuO_x NPs. This work evidenced that copper clusters on titania (constituted by a few number of Cu atoms) were not appropriate for O_2 activation in agreement with DFT calculations. However, for CuO_x NPs of *ca*. 2 nm, O_2 is transformed into peroxo species at the nanoparticle surface (based on *in situ* Raman and IR studies), being active intermediates for the alkyne coupling. Bigger CuO_x NPs led to the formation of lattice oxygen species, exhibiting a lower activity for the oxidative coupling (Fig. 7). The formation of these oxygen-based intermediates agrees with TPR (Temperature Programmed Reduction) profiles. Therefore, the H_2 consumption was very low for copper clusters compared with copper nanoparticles. Furthermore, when CuO_x NPs of 2 nm were treated with phenylacetylene and $^{18}O_2$ under reaction conditions (90 °C, 1 h), neither $H_2{}^{16}O$ nor $H_2{}^{18}O$ was detected, meaning that the surface was reduced under catalytic conditions but it was not reoxidized, plausible due to the formation of peroxo intermediates; in contrast, for bigger CuO_x NPs, both $H_2{}^{16}O$ and $H_2{}^{18}O$ were detected, indicating a partial reduction and reoxidation by $^{18}O_2$ of the surface, in agreement with O_2 dissociation at the surface transforming into a lattice oxygen species.

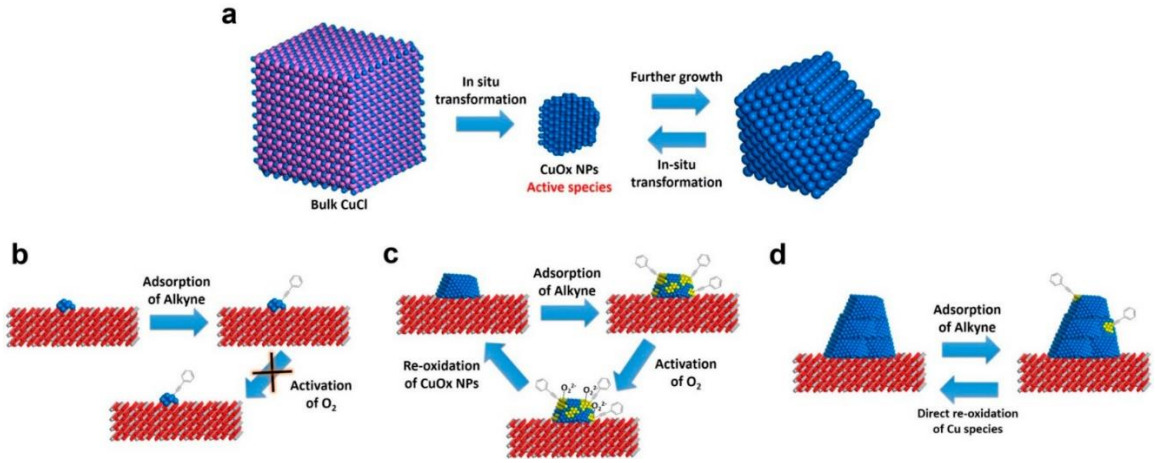

Fig. 7 a) Schematic representation of the transformation of Cu-based species; b-d) Proposed mechanisms depending on the size of the catalytic material: b) CuO_x/TiO_2-0.25%; c) CuO_x/TiO_2-2.5%; d) CuO_x/TiO_2-10%. Reprinted with permission from [75]. Copyright 2016 American Chemical Society.

Zheng and coworkers have recently described the synthesis of hybrid copper-based nanoparticles supported on reduced graphene oxide (rGO), Cu/Cu_2ONPs@rGO.[76] Among the copper catalysts tested for the homocoupling of phenylacetylene including Cu(I) and Cu(II) salts, supported and unsupported Cu-based nanoparticles, the highest activity was obtained with Cu/Cu_2ONPs@rGO, which was also efficient for the symmetrical coupling of different terminal alkynes (12 examples), being more active for aryl derivatives. Previous works of the same group using homogeneous catalysts proved the reduction of Cu(II) into Cu(I) by terminal alkynes (XANES, EXAFS and EPR studies)[77] and the synergy between Cu(II) and Cu(I) evidenced by experimental (IR, EPR, XAS) and theoretical (DFT calculations) means.[78] Based on that, authors extrapolated the homogeneous reactivity to Cu/Cu_2ONPs on rGO, conductor support exhibiting a high specific surface, and proposed the mechanism illustrated (Fig. 8).[76] A first π-π interaction between terminal alkyne and rGO layers promotes the alkyne interaction with copper nanoparticles, which, in the presence of a base, leads to the activation of C-H bond and the corresponding formation of Cu-alkynyl intermediates; the synergy between close copper species favors the oxidative coupling and the reduction of copper nanoparticles, subsequently oxidized by molecular oxygen.

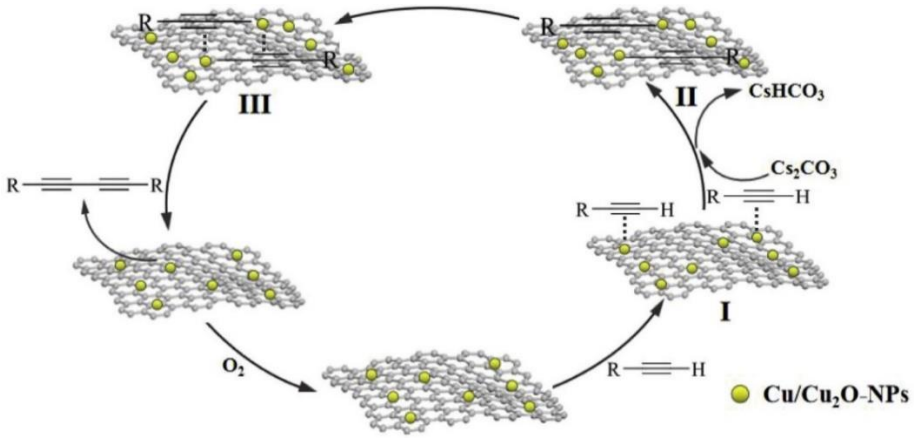

Fig. 8 Plausible mechanism for Glaser homo-coupling catalyzed by Cu/Cu_2O NPs@rGO. Reproduced from [76] with permission of Elsevier and Copyright Clearance Center (license number: 5147061417629) 2019.

Corma's group studied the mechanism of base-free symmetrical homo-coupling of terminal alkynes catalyzed by AuNPs and clusters, both unsupported and supported catalysts on ceria, with the aim of determining the nature of the gold active sites.[70] DFT calculations showed that phenylacetylene can be adsorbed at Au(0), $Au^{\delta(+)}$ and Au^{+} sites; the basic oxygen atoms of the support permit its deprotonation (Fig. 9). Moreover, the alkynyl groups bonded to cationic gold atoms are more reactive than those linked to Au(0), and in consequence the activation barriers for the bimolecular coupling step are lower for AuNPs involving a cationic surface. Moreover, kinetic data indicated that the dissociation of molecular oxygen on AuNPs was the rate determining step, corroborated by the theoretical calculations.

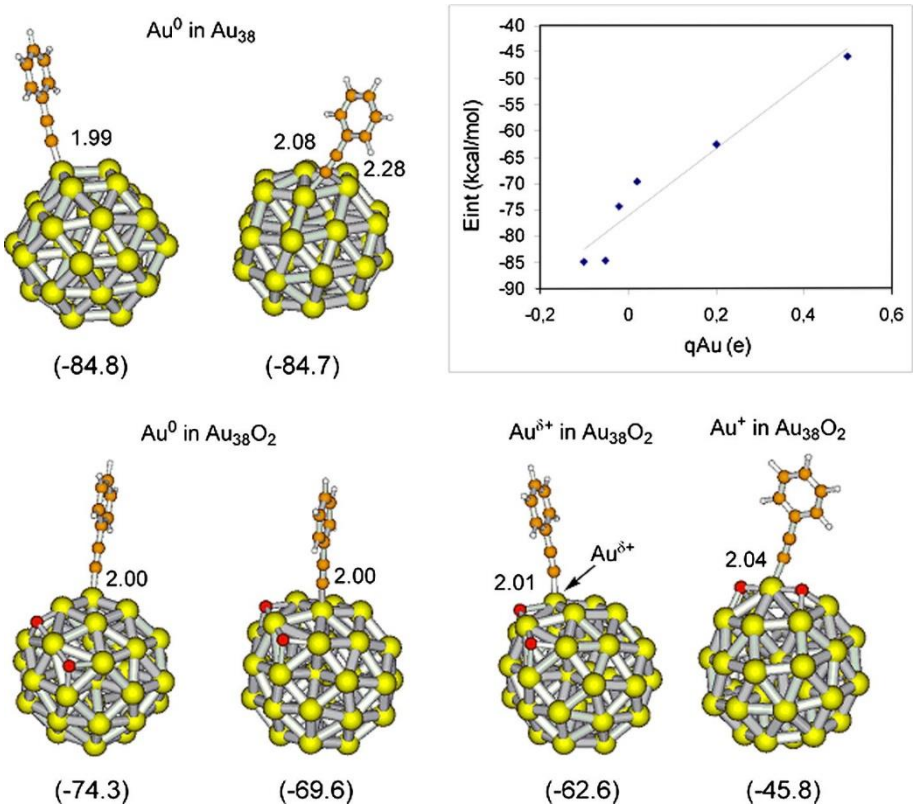

Fig. 9 Interaction of phenylacetylenyl radical with Au(0) and cationic gold (both $Au^{\delta+}$ and Au^{+}) sites on isolated AuNPs. Relationship between calculated energies (data in brackets, kcal/mol) and atomic charge on gold atoms. Metal-carbon distances in Å. Reproduced from [70] with permission of Elsevier and Copyright Clearance Center (license number: 5147070651959) 2014.

Zhang et *al*. proved that Ag(111) surface promotes the C(sp)-H bond activation and the subsequent formation of the corresponding homocoupling product by STM analyses together with DFT calculations, using 1,3,5-triethynylbenzene and 1,3,5-tris-(4-ethynylphenyl)benzene as terminal alkynes.[79]

2.4. Guerbet reaction

The tandem multi-step Guerbet reaction (involving dehydrogenation/aldol condensation/crotonisation/hydrogenation reactions) is an attracting process for the synthesis of branched monoalcohols, value added compounds for industrial production of plasticizers and detergents, including the synthesis of bioalcohols (Fig. 10);[80,81] further hydrodeoxygenation of the obtained branched alcohols makes it possible the production of branched hydrocarbons, components of aviation fuels.[82]

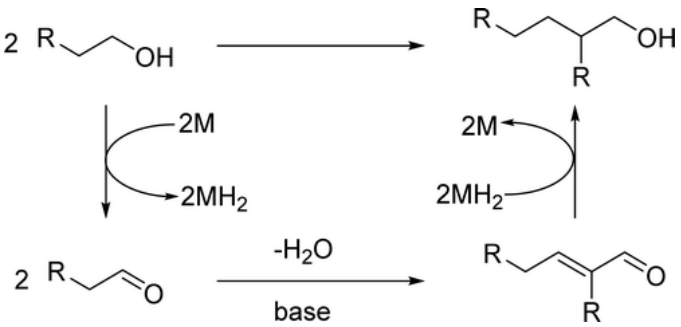

Fig. 10 Schematic representation of Guerbet reaction. Reprinted with permission from [81]. Copyright 2016 American Chemical Society.

Although catalysts consisted of a basic metal oxide (such as MgO) have been widely studied, those composed of a transition metal supported on a basic solid, have received less attention, in particular from a mechanistic point of view. The presence of a transition metal mostly favors the dehydrogenation step of the starting alcohol, permitting to work under lower temperature compared to metal oxides and in consequence avoiding undesired by-products.[83]
Simakova and coworkers have studied the n-pentanol coupling with different platinum-group metals (Ru, Rh, Ir, Pd, Pt) supported on a variety of solids (C, Al_2O_3, TiO_2, CeO_2, ZrO_2) doped with solid bases.[84] These transition metals, in particular Pd and Pt, easily adsorb molecular and atomic hydrogen, promoting the first (alcohol dehydrogenation) and last step (crotonaldehyde hydrogenation). HRTEM (High Resolution Transmission Electron Microscopy) analyses of the as-prepared catalysts showed the presence of small and well-distributed MNPs (mean size 1.0-1.5 nm, except for Pd which exhibits an average particle size of 2.3-2.9 nm). For a given metal, the conversion and selectivity increased with the basic properties (proton affinity) of the support (TiO_2 < ZrO_2 < C < Al_2O_3). For catalysts containing carbon support, the conversion increased as follows: Ir < Ru < Pt < Pd, being PtNPs@Al_2O_3 doped with NaOH (named NaOH/Pt/γ-Al_2O_3) the most selective catalyst towards the formation of 2-propylheptanol. Diffuse Reflectance Infrared Fourier Transform (DRIFT) spectra of adsorbed ethanol on NaOH/Pt/γ-Al_2O_3 permitted to identify the formation of intermediate compounds produced in the Guerbet reaction. Therefore, at room temperature, the formation of acetaldehyde and hydroxyaldehyde could be inferred; after heating at 100 °C, new bands appeared corresponding to the formation of crotonaldehyde. These spectroscopic data corroborate the dehydrogenation/aldol condensation/hydrogenation steps according to a hydrogen borrowing reaction mechanism.

3. C-C CROSS-COUPLING REACTIONS

Since 1960's, C-C cross-coupling reactions, in particular applied in organic synthesis, are generally related to palladium-catalyzed transformations, recognized with the Nobel Prize in Chemistry 2010 conferred to R. F. Heck, E.-I. Negishi and A. Suzuki. In this section, we focus on mainly Pd-based nanoparticles (both mono- and bimetallic nano-catalysts) applied in C-C bond formation transformations, works including fundamental insights regarding surface reactivity based on experimental and in some cases also computational data.

3.1. Sonogashira coupling

Palladium-based catalysts in the presence or in the absence of Cu(I) salts (acting as cocatalyst and thus enhancing the reaction rate), have found a remarkable success in C(sp^2)-C(sp) cross-couplings of aryl or alkenyl halides or triflates and terminal alkynes,[85-87] leading to aryl-alkynes and conjugated enynes, intermediates particularly involved in the synthesis of drugs, natural products and organic materials.[88] Other than molecular catalysts, preformed Pd-Cu BMNPs have been employed in Sonogashira couplings, both BMNPs dispersed in liquid phases and immobilized on solid supports.
Related to colloidal BMNPs, our group prepared Pd-Cu BMNPs by a co-reduction approach in glycerol under hydrogen atmosphere using different Pd/Cu ratios. Those obtained from an equimolar Pd/Cu ratio exhibited a cluster-in-cluster structure [evidenced by HAADF (High-Angle Annular Dark Field)-STEM and EDX (Energy Dispersive X-ray analysis) line scanning]. The as-prepared BMNPs were successfully applied in the synthesis of functionalized triazoles through one-pot tandem reaction, *i.e.* azide alkyne cyclisation coupling followed by Sonogashira reaction; this process displayed an excellent chemoselectivity due to the significant different rates of both processes (Cu-catalyzed triazole formation was faster than Pd-catalyzed C-C bond formation).[89] Domingos and coworkers synthesized core-shell Pd-Cu BMNPs in ethylene glycol/water by a polyol methodology.[90] Based on kinetic profiles, poisoning experiments (Hg, CS_2) and hot filtration tests, authors evidenced that both aryl halide and alkyne activation took place at the BMNP metal surface. However, HRTEM analysis after catalysis showed a significant size decrease of nanoparticles (from 3.8 to 2.8 nm, before and after catalysis respectively), pointing to a plausible metal leaching from the surface; this assumption was also supported by HRMS analysis which proved the presence of molecular copper acetylide species in the catalytic mixture. Therefore, after the oxidative addition to Pd(0) by the aryl halide and the formation

of the alkynylcopper at the BMNP metal surface, a lixiviation of both palladium and copper species occurred before the transmetalation elemental step which occurred in solution (Fig. 11). These facts are in agreement with the Pd lixiviation after the oxidative addition on the metal surface proposed by Rothenberg and coworkers, for copper-free Pd-catalyzed Sonogashira coupling using palladium clusters as catalyst precursor.[91]

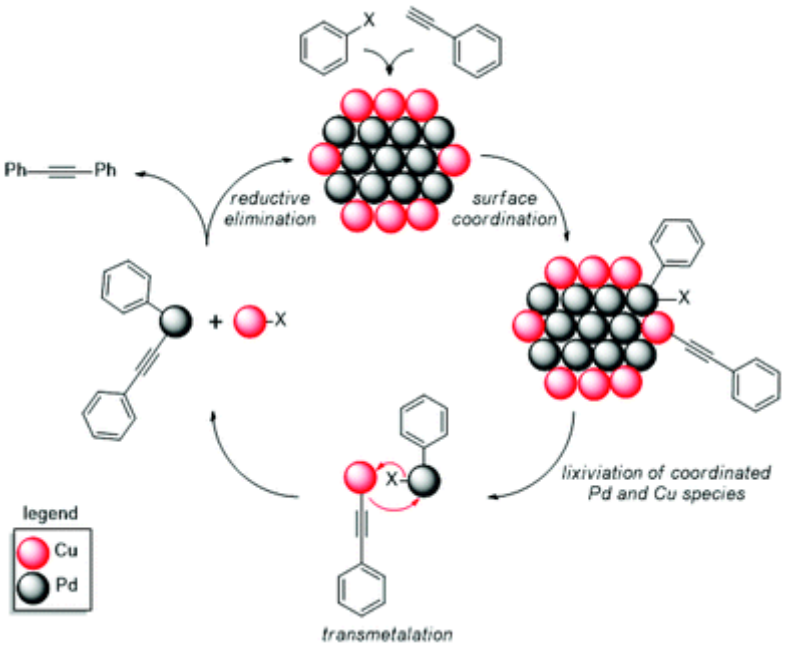

Fig. 11 Plausible mechanism for Sonogashira cross-coupling catalyzed by PdCu bimetallic nanoparticles. Reproduced from [90] with permission from the Royal Society of Chemistry.

Concerning Pd-Cu BMNPs immobilized on supports, Zhang, Gao and co-workers prepared well-defined Pd-Cu nanoalloys on montmorillonite, constituted of Pd(0) and Cu(I) (XPS analyses).[92] Catalytic materials containing Pd-Cu BMNPs of 10-11 nm (mean diameter) showed high activity and chemoselectivity in the coupling between aryl iodides and terminal alkynes, compatible with different types of functional groups. The synergistic effect between both metals was inferred by the dramatic decrease in activity when an equimolar amount of monometallic nanoparticles supported on montmorillonite was tested (from 97% to 26% yield for Pd-Cu nanoalloys and mixture of monometallic nanoparticles, respectively). Similar catalytic behavior was also observed for Pd-Cu nanoalloys anchored on graphene oxide.[93]

Regarding gold-based catalysts, Lambert and co-workers demonstrated that supported zero-valent gold nanoparticles catalyzed the cross-coupling between iodobenzene and phenylacetylene,[94] in contrast to the lack of activity shown by Au(I) and Au(III) supported materials.[95] It was proven that some leaching of ionic gold species into the liquid phase during the coupling happened, but this phase did not exhibit any catalytic activity, indicating that the Sonogashira reaction shows a surface-like reactivity. Furthermore, relative large AuNPs were more active than smaller ones pointing to the need that both molecules, iodobenzene and phenylacetylene, may be adsorbed on large facet planes; small AuNPs (<2 nm) favored the formation of biphenyl (homo-coupling process).[96] The same authors observed a similar trend using RhNPs supported on both γ-alumina and BaO.[97]

Regarding the nature of the gold sites, Corma and co-workers studied the Sonogashira coupling by both experimental (kinetic study) and theoretical (DFT calculations) means, using AuNPs supported on lanthanide oxides, such as La_2O_3 and CeO_2 due to their higher selectivity towards the cross-coupling product than those immobilized on silica, alumina or titania, which favor the homocoupling of iodobenzene.[98] This study evidenced that iodobenzene dissociates on Au(0) sites while phenyacetylene is activated on $Au^{\delta(+)}$ ones, being the bimolecular surface elementary reaction the rate determining step. XPS analyses corroborated the presence of both neutral and ionic gold sites in the Au-based

catalysts mainly favoring the cross-coupling reaction, in contrast to those promoting the formation of biphenyl (only Au(0) present in the nanoparticles).

3.2. Suzuki-Miyaura coupling

Initially described in 1979 and 1986, the Pd-catalyzed Suzuki–Miyaura cross-coupling pioneered in the formation of new $C(sp^2)$-$C(sp^2)$ and $C(sp^2)$-$C(sp^3)$ bonds, respectively, from aryl halides and boronic acid substrates.[99,100]

Among all nanocatalyzed Suzuki–Miyaura cross-coupling reactions reported thus far in the literature, most of the works use either monometallic or bimetallic Pd catalyst systems. Thus, this review article will not only take advantage of the level of maturity reached in palladium nanoparticle catalysis to highlight surface mechanistic insights, but also detail the contributions of other transition metals from groups 8 to 10 enabling novel methodologies for the formation of C-C bonds. The key activation of aryl halides in Suzuki–Miyaura cross-coupling reactions has been classically described as an elementary oxidative addition of an aryl halide to a zero-valent Pd center taking place under a homogenous regime. However, nanocatalyst-enabled surface activation mechanisms of aryl halides substrates may differ from classical ones, as reported by Corma, García and co-workers for a catalytic system featuring small-sized nanoparticles that facilitated the oxidative addition via the formation of aryl Pd(II) intermediates.[101] In addition, substrate coordination on the metallic surface and steric effects can strongly tune the catalytic reactivity of preformed Pd NPs and favor oxidative addition as shown for 4-bromoanisole.[102] Thus, the aim of this section is to highlight substrate activation pathways taking place on catalyst surfaces via key substrate interactions (Fig. 12).

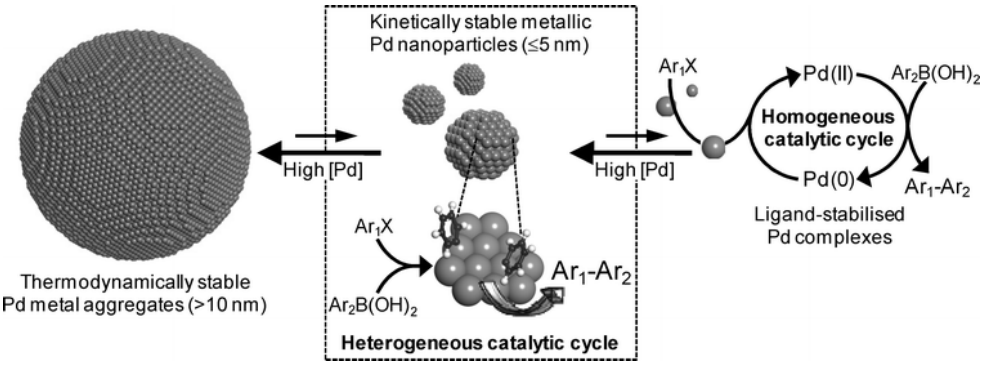

Fig. 12. Plausible reaction manifolds operating in PdNPs catalyzed Suzuki-Miyaura cross-coupling reactions. Reproduced from [103] with permission from the Royal Society of Chemistry, license ID 1149708-1.

Seminal contributions by El-Sayed and co-workers in catalyzed Suzuki-Miyaura cross-couplings with PdNPs stabilized by PVP revealed that an excess of the stabilizer leads to enhanced stability in terms of size and shape due to Ostwald ripening inhibition, albeit on a catalytic activity decrease due to capping of the particle surface.[104] In addition, the boronic acid reagent acts as an stabilizing agent via binding through its boronate groups to the nanoparticle surface (as confirmed by FT-IR),[105] whereas iodobenzene and sodium acetate affected the stability of the nanoparticles by favoring Ostwald ripening via the leaching of molecular palladium species and their re-deposition for the reaction carried out at 100 °C in a MeOH-toluene solvent mixture (Fig. 13). Despite a weak interaction has been described between iodobenzene and the catalyst surface, it is worth to mention that the addition of biphenyl product to the reaction mixture resulted in low conversions via catalyst poisoning. Similar results were obtained by El-Sayed and co-workers for Pd nanocatalysts systems stabilized by polyamidoamine (PAMAM-OH) dendrimers.[106] Besides the size increase of spherical PdNPs catalysts, Ostwald ripening processes can be operative with other catalytic systems as observed for tetrahedral PtNPs systems that grow in size adopting a spherical shape under Suzuki-Miyaura cross coupling conditions.[105]

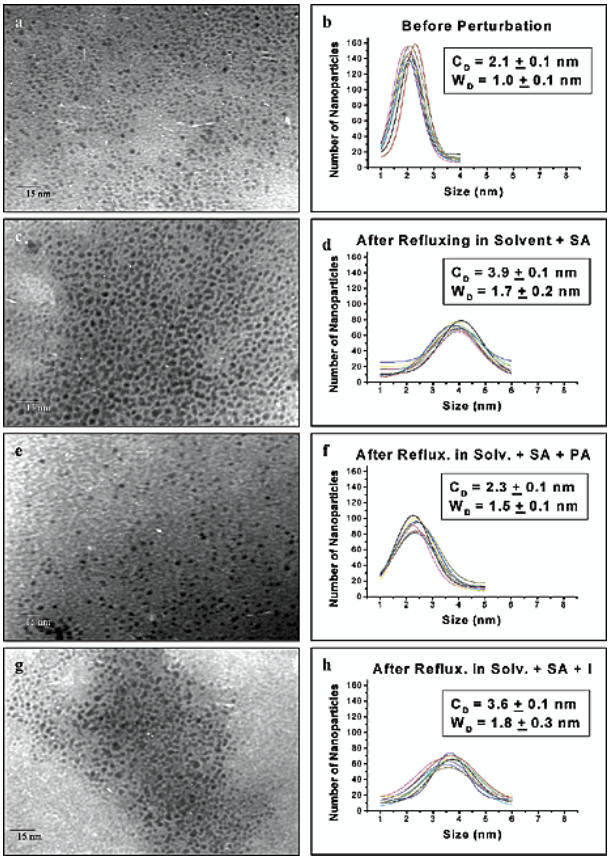

Fig. 13 TEM images and statistical distributions of a, b) preformed PdNPs stabilized with PVP; c, d) after refluxing in sodium acetate; e, f) after refluxing in the presence of sodium acetate and phenylboronic acid; g, h) after refluxing in the presence of NaOAc and iodobenzene. Adapted with permission from [104]. Copyright 2003 American Chemical Society.

The interplay of surface reactivity of Suzuki-Miyaura cross-coupling reaction of iodoanisole and phenylboronic acid with preformed PdNPs has been studied by Lee and co-workers via operando liquid-phase XAS monitoring (Fig. 14a-e).[103] Under their operando conditions (using KOMe as base at 60 °C in a MeCN-H_2O solvent mixture), no metal leaching was observed, providing novel insights on the direct implication of surface density Pd defect sites in the Suzuki-Miyaura cross-coupling reaction catalyzed by PdNPs (Fig. 14f, size dependent TOF calculated taking into account all surface Pd atoms *versus* a constant TOF normalized to surface defect atoms). In addition, the kinetic profiles evidence a fast reaction without induction period followed by deactivation over time (Fig. 14g).

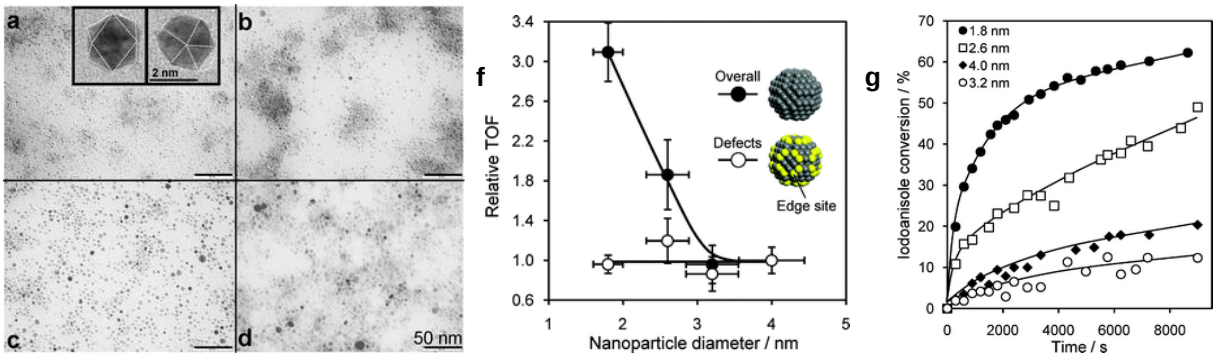

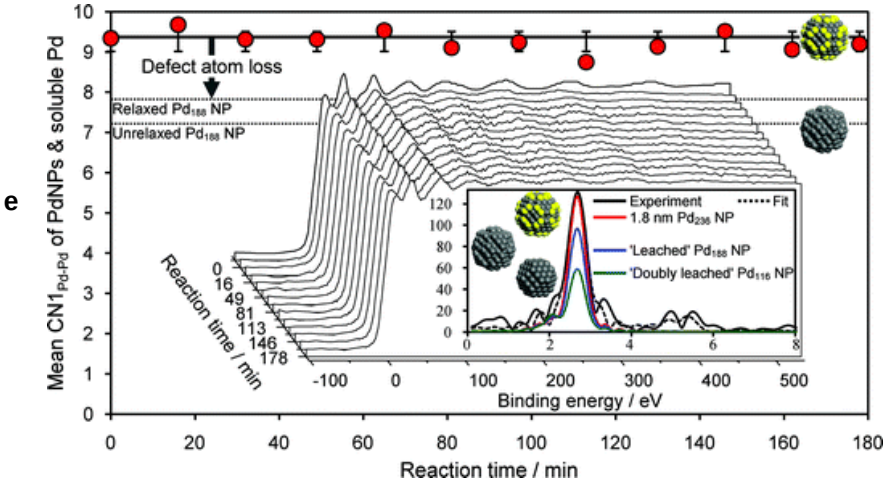

Fig. 14 (a, b, c and d) TEM micrographs of PdNPs stabilized by PVP of the following sizes: 1.8, 2.6, 3.1 and 4.0 nm, respectively, with a high resolution micrograph representative of the surface geometry of a 1.8 nm; (e) Operando Pd K-edge XAS fits for Suzuki-Miyaura reaction monitoring of iodoanisole and phenylboronic acid with 1.8 nm PdNPs stabilized by PVP. Inset represents normalized, time-dependent EXAFS spectra with real/simulated radial distribution functions for different Pd cuboctahedra; (f) Plot of TOFs versus the total (●) or surface atom densities with defects (○) of the largest nanoparticle evidencing the structure-sensitive Suzuki-Miyaura coupling reaction of iodoanisole and phenyboronic acid over PdNPs; (g) Reaction profiles for Suzuki-Miyaura cross-coupling of iodoanisole and phenylboronic acid catalyzed by the as-prepared PdNPs systems. Reproduced from [103] with permission from the Royal Society of Chemistry, license ID 1149708-1.

Given the fact that classical substrate activation pathways via oxidative addition may be implicitly linked to the leaching of molecular species via the oxidation of the metal, finding alternative activation modes is crucial in the quest towards the development of novel catalyst systems with enhanced reactivity and selectivity outcomes. As an example, Kutubi, Kitagawa and Nagaoka reported in 2015 the preparation of a bimetallic catalyst system featuring alloyed $Pd_{0.5}Ru_{0.5}$ NPs stabilized with PVP (Fig. 15), exhibiting dual Lewis acidic/basic properties that facilitate the oxidative addition via the intrinsic charge density transfer from Pd towards Ru as evidenced by XPS characterization: +0.25 eV positive binding energy shift for Pd $3d_{5/2}$ (334.55 eV) together with a -0.80 eV negative binding energy shift for Ru $3p_{3/2}$ (460.60 eV) in comparison to analogous monometallic Pd and Ru NPs systems stabilized by PVP (334.30 and 461.4 eV, respectively).[107] The synergistic effects of alloyed PdRu NPs cooperatively participate in the activation of both Suzuki-Miyaura polar substrates via a rapid cleavage of haloarene C–X and boronic acid C–B bonds, yielding the formation of arylruthenium and arylpalladium species, respectively, in neighboring disposition that allow a reductive elimination to deliver the cross-coupled biphenyl product (Fig. 16).

Furthermore, a series of analogous bimetallic $Pd_{74}M_{73}$ (M = Cu, Pt, Au, Rh, Ru) dendrimer encapsulated NPs were synthesized by Tang, Shi, Hu and co-workers and their catalytic performance towards the Suzuki-Miyaura cross coupling was assessed. Both Pd_{147} and $Pd_{74}Cu_{73}$ nanocatalyst systems furnished high yields (>79%) after short reaction times (45 min), and high TOFs (>8519 h^{-1}).[108] Despite comparable energy barriers concerning the rate-determining step were determined for both monometallic Pd_{147} and bimetallic $Pd_{74}Cu_{73}$ dendrimer encapsulated NPs systems, substrate adsorption energies on the latter are slightly lower than those for monometallic ones. PdCu synergistic effects were assessed by DFT calculations, showing electron density differences that correlated nicely with a model encompassing the transmetalation of boronic acid at Cu sites on the catalyst surface, boosting the Suzuki coupling reaction.[108]

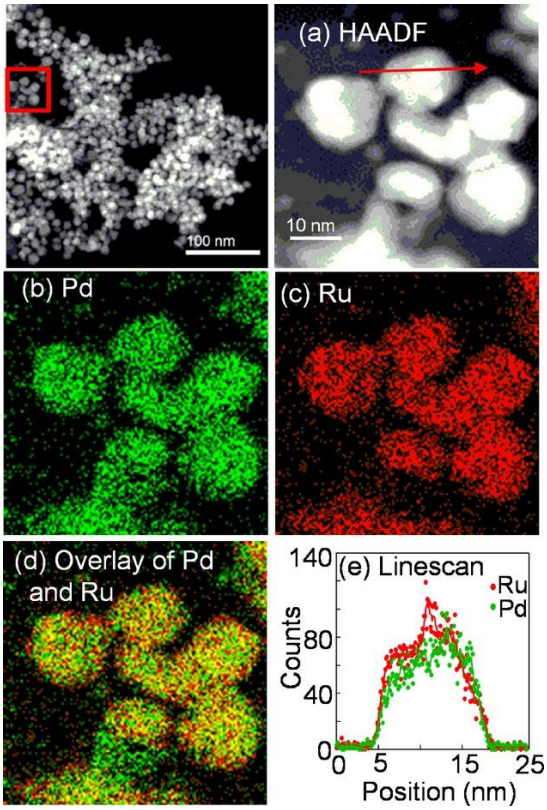

Fig. 15 HAADF–STEM image of bimetallic $Pd_{0.5}Ru_{0.5}$ NPs stabilized with PVP after three runs of Suzuki-Miyaura coupling reaction and TEM–EDS analyses of the area framed with a red line. a) HAADF–STEM image; b–d) EDS mapping for Pd (green), Ru (red) and its overlay showing the co-localization of both metals in yellow; e) linescan profile along the arrow in (a) Pd (green) and Ru (red). Reproduced from [107] with permission of John Wiley and Sons and Copyright Clearance Center (license number: 5153740025431) 2015.

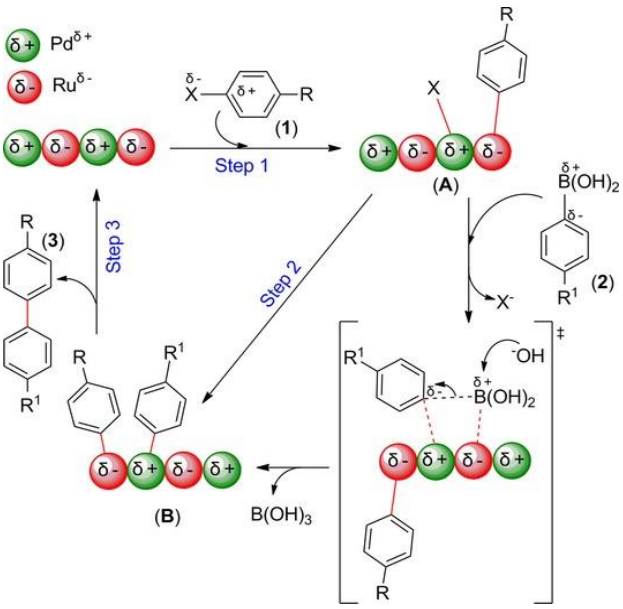

Fig. 16 Plausible mechanism for the Suzuki-Miyaura coupling catalyzed by a bimetallic $Pd_{0.5}Ru_{0.5}$ NPs system with PVP as stabilizing agent. Reproduced from [107] with permission of John Wiley and Sons and Copyright Clearance Center (license number: 5153740025431) 2015.

Catalyst heterogenization on both inorganic oxides (SiO_2, Al_2O_3, zeolites) or polymeric organic materials with special emphasis on entrapped nanoparticles in polymeric matrixes is an actively sought strategy as it represents a viable strategy towards catalyst enhancement via synergistic effects

between metal NPs and the supports, as well as facilitated catalyst recovery and reuse.[109,110] Gupton, Khanna and co-workers have recently reported computational and experimental results shedding light on the nature of interfacial interactions between metal NPs and defect sites on a graphene surface.[111] The authors describe not only that the void sites on the surface of graphene provide enhanced stability against metal leaching through strong binding of the metal clusters, but also this support facilitates specific steps in the catalytic cycle, such as the oxidative addition via electron density transfer processes to the metal cluster, thus lowering the activation energy barrier of Suzuki cross-coupling reactions occurring at Pd@graphene catalyst surfaces (Fig. 17).[111] Furthermore, Blanco, Agnoli and co-workers have recently described a tunable methodology for the synthesis of size-controlled PdNPs (ranging from 1 to 9 nm) on graphene acid via impregnation of the support with $Pd(OAc)_2$.[53]

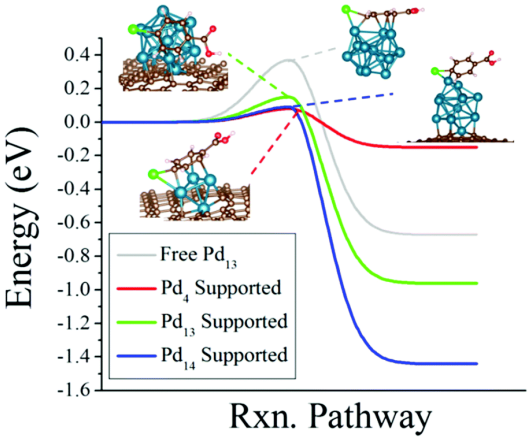

Fig. 17 Reaction pathway for oxidative addition of bromobenzoic acid on a Free Pd_{13} cluster, and supported Pd_n clusters on defected graphene, n=4, 13, and 14. Reproduced from [111] with permission from the Royal Society of Chemistry, license ID 1148395-1.

A similar activation mode via electron density donation to the metal sites has been described by Qu and co-workers for catalytic systems featuring PdNPs supported on porous CeO_2 nanorods. The reported nanocatalysts composites can accelerate the initial oxidative addition step thanks to strong Pd-support interactions (Fig. 18), namely Pd sites enriched in electron density in combination with the strong basicity and a high number of oxygen vacancies in the CeO_2 supports, as evidenced by a binding energy increase in core level Pd3d peaks in XPS (Fig. 18f).[45] The formation of reactive "ArPd(II)Br" species is proposed, but the authors do not comment whether the nature of the reactive intermediates is molecular or adsorbed on the catalyst surface.[45] Analogous synergistic effects have also been described by Ye and co-workers for highly active core-shell microspheres, bearing a magnetic Fe_3O_4 core, a layer of PdNPs and an outer shell of mesoporous CeO_2.[112]

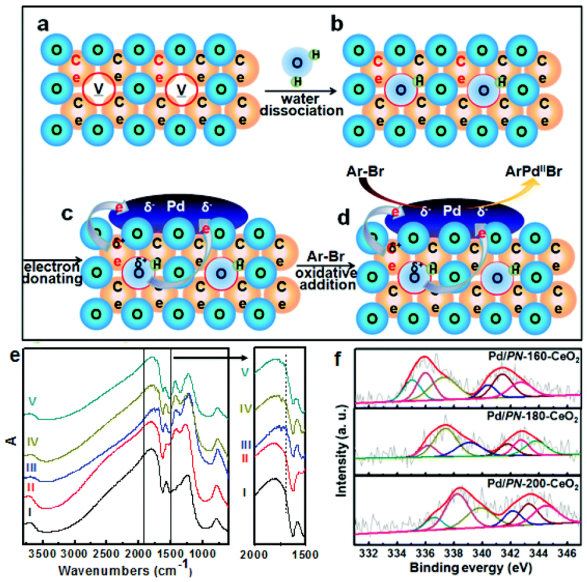

Fig. 18 (a, b, c and d) Proposed mechanism for the Suzuki-Miyaura cross-coupling catalyzed by PdNPs@CeO_2; (e) FT-IR spectra of a series of PdNPs@CeO_2 catalysts; (f) XPS analysis of Pd nanocatalysts. Reproduced from [45] with permission from the Royal Society of Chemistry, license ID 1148288-1.

The preparation of highly active catalytic materials with enhanced reusability properties has also been enabled by the immobilization of PdNPs on solids supports such as silicates (mesoporous SiO_2,[113,114] mercaptopropyltrimethoxysilane-SiO_2,[115] PEG-SiO_2,[116] silicalite-1,[117] montmorillonite[47]), $ZnAl_2O_4$ spinel,[118] ferrite,[119] magnetite,[120,121] chalcogels,[122] covalent organic frameworks,[123-125] metal organic frameworks (Eu-MOF,[126] MCM-41,[127] MOF-5,[128,129] MIL-101,[130] Cu-MOF,[131]) Carbon-based materials (graphene,[111] graphene oxide,[132-134] graphene acid,[53] Carbon nanotubes[135]), polymeric matrixes [dendrimers,[108] poly(amido-amine) (G4-PAMAM),[106] 2-aminobenzaldehyde modified chitosan nanofibers,[136] DIANION,[137] mesoporous polyaminophenols,[138,139] poly(ethylene glycol)-co-poly(*N*-isopropylacrylamide),[140] nylon rope[141]], or composite materials of mixtures thereof.[142-147]
Literature reports on surface-like Suzuki-Miyaura cross-couplings under aerobic conditions address the challenge of precluding boronic acid homo-coupling, a competing side reaction occurring in the presence of O_2 via the formation of palladium(II) peroxo species[148] that can easily undergo two successive transmetallations with boronic acid substrates as aryl halide oxidative addition to Pd(0) is the rate determining step under classical molecular regimes.[149-151]

Solvents exhibiting low solubility profiles for O_2 or heterogeneized systems capable of precluding Pd oxidation under aerobic conditions might enable selective and sustainable Suzuki-Miyaura cross-couplings precluding homo-coupling reaction manifolds. The results of Ma and co-workers[120], Wang and co-workers[130], Ye and co-workers[112] provide nice examples of selective nanocatalysts systems operating in air, but further studies the operating catalytic reaction via precluding molecular homo-coupling reaction manifolds merits further studies.
Suzuki carbonylative coupling reaction is one of the most facile and effective routes for direct synthesis of biaryl ketones from carbon monoxide, aryl halides and arylboronic acids, with various functionalities. Recently, Hajra et *al.* reported the past decades developments in the carbonylative Suzuki-Miyaura carbonylative coupling reactions using modern methods based on transition-metal catalysts with special emphasis to Pd.[152] Also, Vessally and coworkers reviewed recent progress in the application of NPs for carbonylative Suzuki coupling.[153] Among different systems, the immobilization of Pd species on inorganic nanoparticles present interesting catalytic activities for the studied reaction. Thus, different works reported the preparation of functionalized nano-objects to stabilize Pd(II)-complexes or PdNPs. By varying arylboronic acids and aryl iodides groups, the reaction mechanisms were proposed in literature for Fe_3O_4/L-Pd^n catalysts (where L is stabilizing agent, as ligands or

polymers, *n* = 0, 2).[154,155] Moreover, Ma and coworkers demonstrated that Fe_3O_4/L-Pd(0) (L = dopamine) system exhibits much inferior catalytic performance than Fe_3O_4/L-Pd(II). Such catalytic behavior could be ascribed to the fact that PdNPs are prone to agglomeration reaction. To prove this conjecture, TEM analyses for Fe_3O_4/L-Pd^0 and Fe_3O_4/L-Pd^{II} after Suzuki carbonylative cross-coupling reaction have been performed. The agglomeration was obviously observed by TEM analyses of the catalyst after one reaction. After 5 cycles, very strong aggregation of PdNPs allowed to conclude that the nanosystem based on supported Pd^{II} species is more stable than zero-valent PdNPs.
The research maturity of Pd nanocatalysts reached thus far has fostered the research on selective Suzuki-Miyaura catalysts of other transition metals at the nanometric scale such as PtNPs,[105,156], Au NPs[157-160] and Ru NPs[107,161] and bimetallic systems thereof[107,157,158,162] with light-tunable surface plasmon reactivity.[157] However the impact of abundant first-row transition metals as key enablers towards new sustainable chemical paradigms is foreseen in the years to come. Notably, catalyst nancomposites featuring Ni NPs[163], Ni_xOy NPs,[164] Co NPs[165] or Co(II) complexes,[166], or bimetallic Co-Cu systems have recently been described.[167]

3.3. Dehydrogenative cross-couplings

Dehydrogenative cross-coupling (DCC) offers a unique way of C−C or C−X (X = heteroatom) bond formation reactions. Numerous reviews have been published on such reactivity catalyzed by transition metal complexes, metal nanoparticles, and metal-free systems.[168,169] The application of nanocatalysts in cross-dehydrogenative coupling reactions has been recently reviewed by Vessally and co-workers.[170]
A photocatalytic DCC reaction mechanism was proposed for hybrid materials combining noble metal NPs (*e.g*. Pt, Pd or Au-Pd bimetallic NPs) and semiconductor metal oxides (*e.g*. TiO_2, CeO_2).[49,171,172] The proposed mechanism takes place as follows: *(i)* semiconductor metal oxide is excited by photo-irradiation to generate the hole and electron; *(ii)* then transferred to metal NPs; *(ii)* hole would activate the organic molecules (*e.g*. C-H bond) to generate radical and a proton; *(iii)* the organic radicals combine to give a final product; *(iv)* the protons are reduced by the electrons migrated from semiconductor to MNPs to form H_2.
Yoshida *et al*. studied the DCC reaction between toluene and acetone catalyzed by MNPs@TiO_2 (where M = Pd, Pt), carrying out different experiments with the aim of understanding the process, including EPR analyses (identification of radicals), kinetic experiments, and temperature-controlled photocatalytic tests.[171] Based on these observations, two catalytic mechanisms were proposed (Fig. 19) showing the importance of the metal NPs cocatalyst nature on the selectivity of the DCC products. Thus, the high activation energy for 1-(o-tolyl)propan-2-one determined from pseudo-Arrhenius plots of the temperature-controlled photocatalytic tests, suggests the involvement of a certain non-photocatalytic process for PdNPs@TiO_2 system. The authors proposed that PdNPs promote the DCC between toluene and acetone *via* radical addition-elimination mechanism. On the other hand, the weak activation energy determined for PtNPs@TiO_2 indicates that PtNPs contribute as an electron receiver and promote the DCC reaction between the methyl group of toluene and acetone through a radical-radical coupling.

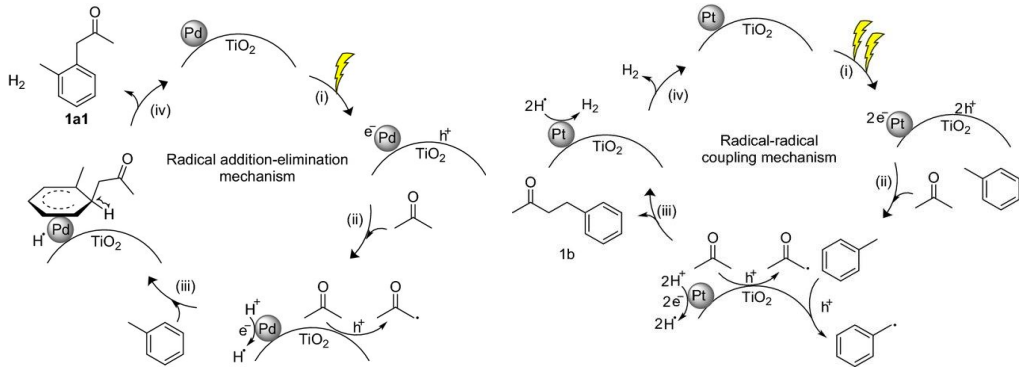

Fig. 19 Proposed mechanisms for the photocatalytic DCC between toluene and acetone catalyzed by PdNPs@TiO_2 (left) or PtNPs@TiO2 (right). Reprinted from [171] with permission from Springer Science Business Media, LLC, part of Springer Nature 2019.

To avoid the possible alternation of the metal co-catalyst part on the TiO_2 surface, a design of blended catalyst has been proposed by the same group, consisting in a physical mixture of a TiO_2 photocatalyst and MNPs supported on Al_2O_3.[49] The advantage of this system is the possibility to finely tune the catalytic properties of two catalysts to achieve high activity. Firstly, by examining the DCC of benzene and THF with different catalysts (*i.e.* Pd@TiO_2, Pd@Al_2O_3, TiO_2, TiO_2 + Pd@Al_2O_3), the authors showed that PdNPs can work more efficiently if they are not directly supported on TiO_2. However, the coexistence TiO_2 component is essential to promote the DCC reaction. Thus, it was demonstrated that modification of one of the catalytic components, such as the insertion of small amount of Au to Pd@Al_2O_3 system, increased the blended catalyst activity and selectivity for the photocatalytic direct DCC between arenes and THF. The observed behavior was related to the electron deficient Pd species in $Pd^{\delta+}$-$Au^{\delta-}$ nanoparticles, suggested by Au L_{III}-edge XANES analyses, which can withdraw the electron density from an adsorbed arene to accelerate the reaction with a THF radical. This step is crucial for the proposed DCC reaction mechanism (Fig. 20).

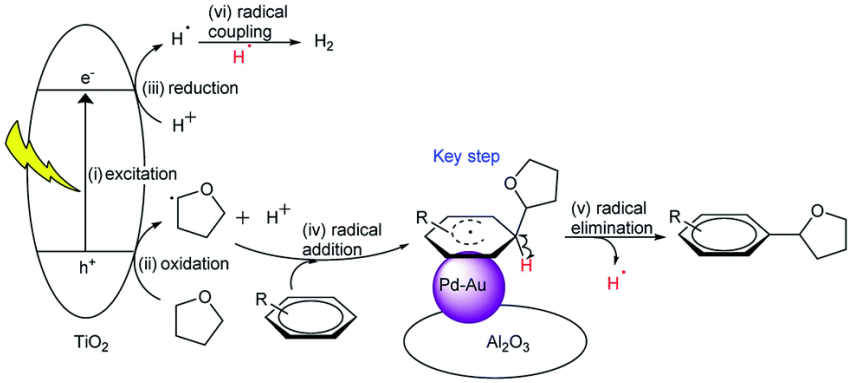

Fig. 20 Proposed mechanism for the photocatalytic DCC between arenes and THF by the blended catalyst consisting of TiO_2 photocatalyst and Pd-AuNPs@Al_2O_3. Reproduced from [49] with permission from the Royal Society of Chemistry.

Alonso's group studied CuNPs on zeolite Y to catalyze DCC of tertiary amines with terminal alkynes in the presence of tert-butylhydroperoxide (TBHP) as oxidant to yield propargylamines.[173] The authors showed that the mechanism involves radical species and the couple Cu(I)/Cu(II) (Fig. 21 Top). To demonstrate this, several experiments were carried out, one of them using a radical scavenger that inhibited the propargylamine formation (especially with TEMPO). Thus, the formation of acetone from TBHP was observed by adding 2,4-dinitrophenylhydrazine to obtain the corresponding hydrazone under the reaction conditions (70 °C, 5 h, solvent-free) even without catalyst. Concerning the catalytic material, the authors performed XPS analysis for CuNPs after catalysis Cu($2p_{3/2}$) peaks (Fig. 21 Bottom). CuNPs showed 4 peaks corresponding to Cu_2O, CuO and two other satellite peaks corresponding to Cu^{2+} species. After catalysis, Cu(II) species disappeared and the sample was mainly constituted of Cu_2O. After oxidative treatment with TBHP, the starting CuNPs were regenerated, showing that the Cu(II) species play a crucial role in DCC.

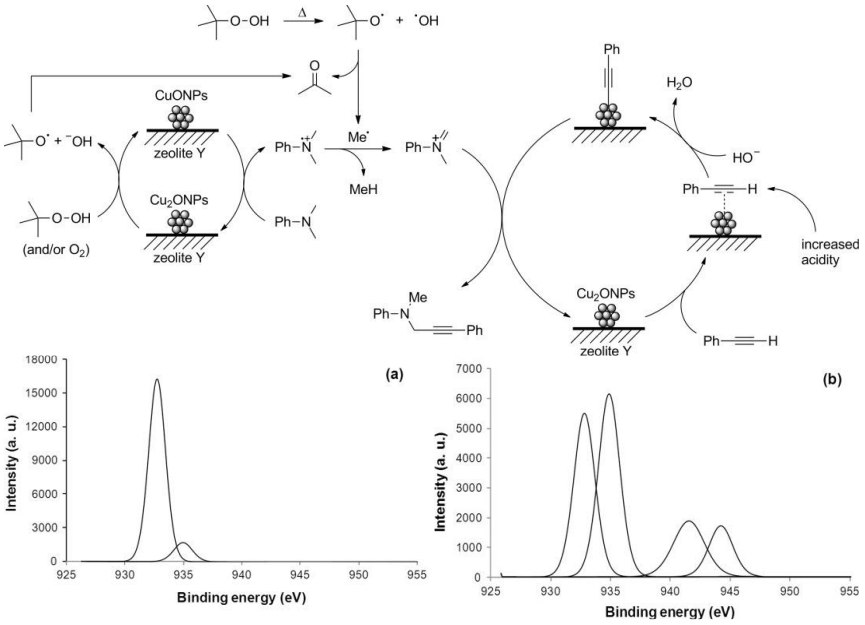

Fig. 21 (Top) DCC reaction mechanism between *N*,*N*-dimethylaniline and phenylacetylene catalyzed by CuNPs@ZY in the presence of TBHP. (Bottom) XPS spectra of CuNPs@ZY at the Cu $2p_{3/2}$ level at the end of the DCC (a) and after reoxidation (b). Reproduced from [173]. Copyright 2015 Wiley-VCH Verlag GmbH & Co. KGaA, Weinheim.

Based on these results, the following mechanism was proposed: *(i)* the Cu(I) phenylacetylenide complex is formed from the Cu_2ONPS and phenylacetylene; *(ii)* in parallel, the decomposition of TBHP occurs, leading to terbutoxyl and hydroxyl radicals, and further to methyl radicals and acetone; *(iii)* the obtained molecules oxidize Cu_2ONPs into CuONPs and then reduced with the concomitant oxidation the amine in its radical cation; *(iv)* H-transfer between the methyl radical and the radical cation amine give an iminium; *(v)* when iminium is added to the copper phenylacetylenide complex, generation of the propargylamine is observed.

In a similar way, a radical process for DCC reaction between tetrahydroisoquinolines and nitroalkanes was also proposed for Cu-oxide based NPs supported on TiO_2 (Fig. 22).[174] Radical traps and catalyst poisons were used to study the plausible DCC inhibition. XPS studies were performed to demonstrate the strong interaction of CuNPs with the nitro group of nitroalkanes, presumably, promoted by CuONPs.

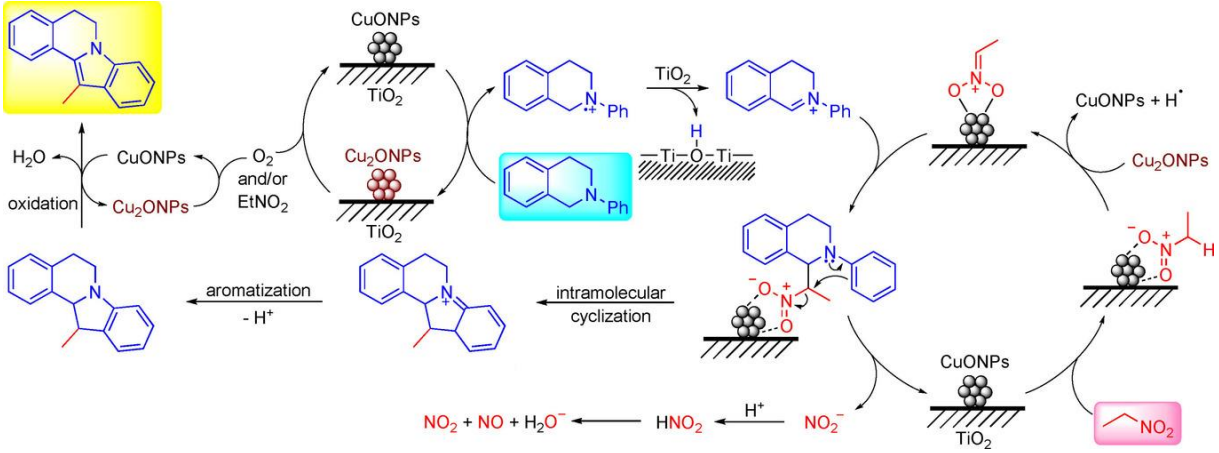

Fig. 22 DCC reaction mechanism between tetrahydroisoquinolines and nitroalkanes catalyzed by $Cu_xONPs@TiO_2$ (x = 1, 2) Reproduced from [174]. Copyright 2018 Wiley-VCH Verlag GmbH & Co. KGaA, Weinheim.

The involvement of metal oxide on the MNPs surface was observed for other catalytic systems. Thus, Loh et coworkers showed that IrO_2 species on the 0.1 wt% Ir@Mg_4AlO catalyst promote the kinetically important step in the DCC of indole and methanol.[175] XRD measurements of the obtained material showed neither IrO_2 and not metallic iridium diffraction pattern in 0.1 wt % Ir@Mg_4AlO. Similarly, XPS studies showed oxidized Ir species detected despite very weak binding-energy peak due to low Ir content. Then, to investigate the catalytic mechanism, time-dependent product evolution for indole-methanol coupling reaction was studied by GC. Different separate experiments showed that the condensations of indole with paraformaldehyde gave the 3,3'-bis(indolyl)methane (3,3'-BIM), suggesting the formaldehyde could be the intermediates in indole–methanol coupling to 3,3'-BIM transformation. It should be note that the selectivity for 3,3'-BIM produced by indole and formaldehyde by adding paraformaldehyde gradually was much higher than by adding paraformaldehyde at one time, indicating the *in situ* formed formaldehyde on 0.1 wt % Ir@Mg_4AlO with low concentration is one of the crucial factors to allow the reaction proceeding in a selective manner. Moreover, isotope labeling study demonstrated the expected deuterium incorporation at the carbon of bridging methylene group, but with low reaction rate. This observation indicates that the dissociation of a C–H and/or O–H in methanol in the first step catalyzed by 0.1 wt % Ir@Mg_4AlO is involved as a kinetically important step (Fig. 23).

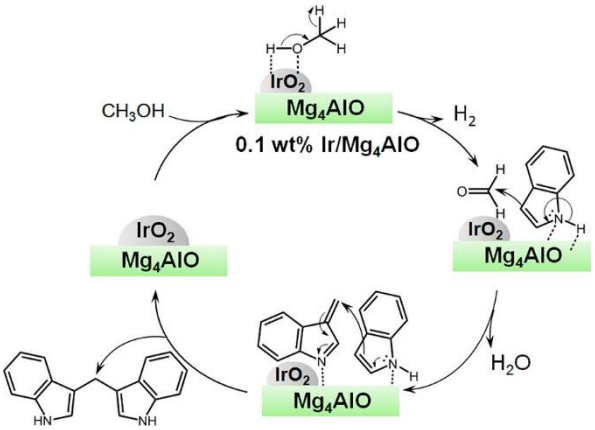

Fig. 23 Schematic representation of DCC reaction mechanism between indole and methanol catalyzed by 0.1 wt % Ir@Mg_4AlO. Reprinted with permission from [175]. Copyright 2019 American Chemical Society.

Characterization and a systematic study of the influence of RuNPs with different oxidation on their catalytic activity in DCC reaction between tetrahydroisoquinolines and nucleophiles (*e.g*. indole or nitromethane) *via* single-electron transfer were performed by Yan and coworkers (Fig. 24).[176] EPR analyses of RuNPs with different content of Ru(III) species were carried out. Samples with a higher content of Ru(III) present the higher catalytic activity due to the generation of superoxo- or peroxo-like species ($*O_2^{\cdot-}$). The content of Ru(III), as well as the oxidation states of Ru and RuO_2 NPs have been investigated by XAFS and XPS. The obtained data showed that Ru(0) was present in RuNPs centers, and in the interface, the oxidized Ru triggered the DCC reaction. Based on these data, a heterogeneous catalytic mechanism was proposed, as well as volcano shaped correlation between the oxidation state of the NPs surface and their catalytic activity was established.

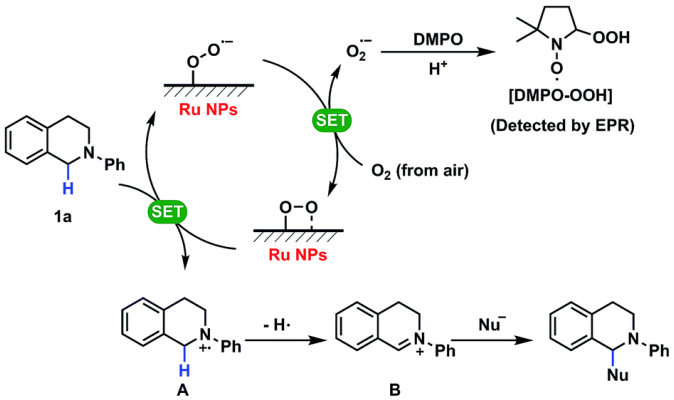

Fig. 24 DCC mechanism between tetrahydroisoquinolines and nucleophiles catalyzed by RuNPs. Reproduced from [176] with permission from the Royal Society of Chemistry.

4 C-heteroatom cross-couplings

Carbon-oxygen and carbon-nitrogen bonds are present in a wide variety of compounds, particularly in biologically active molecules.[177-179] These organic compounds are often synthesized through efficient and low-cost catalytic coupling reactions by the formation of C-X bonds.[180,181] The reactivity comprehension permits the design of selective catalysts and thus leads to sustainable processes.[182]

4.1. C-O bond formation reactions

Friend's group studied the synthesis of esters by vapor-phase cross-coupling of methanol with primary alcohols (such as ethanol and n-butanol) catalyzed by unsupported AuNPs (mean diameter <2 nm).[183] The esterification occurred through activation of alcohols by adsorbed oxygen atoms present on AuNPs by a mechanism involving alkoxy and hemiacetal intermediates. Au(111) surface was oxidized with ozone prior to the reaction with the corresponding alcohols. The slower rate of β-C-H dissociation for methoxy group than that for ethoxy or butoxy groups led to a high selectivity for cross-couplings, efficiently competing with homo-couplings. The mechanism of the coupling reaction of ethanol with methanol was proposed based on different experimental data (Fig. 25): product distribution analysis, isotopic labelling studies showing that the β-hydride elimination occurs from the ethoxy (and not from methoxy), high resolution electron energy loss (HREEL) analyses showing the vibrational mode of methoxy-d_0 and ethoxy-d_5 onto O/Au(111) surface, and temperature programmed heating studies. A similar mechanism was proposed for the coupling of aldehydes with methanol.[184]

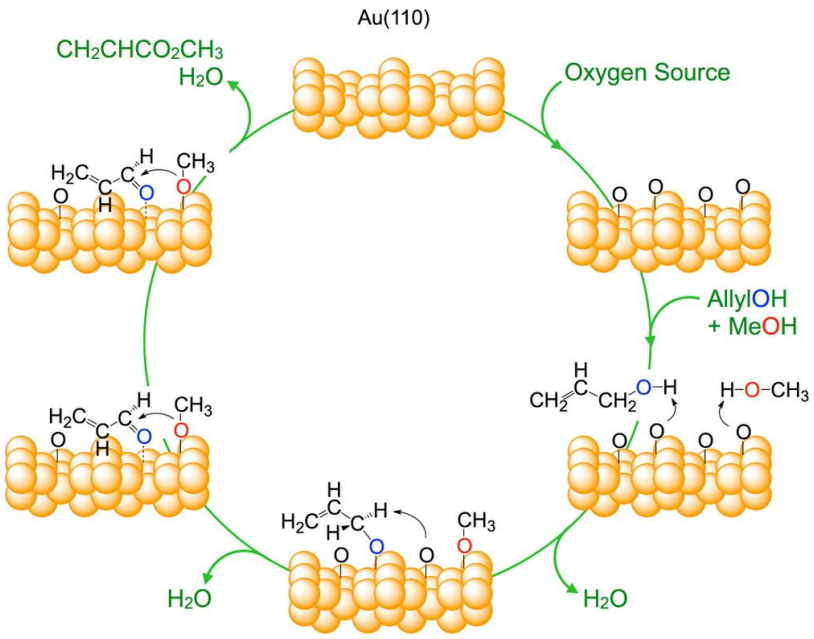

Fig. 25 Mechanism of Allyl Alcohol Coupling with Methanol on oxygen-activated Au(110) surface. Reprinted with permission from [185]. Copyright 2016 American Chemical Society

This mechanism was also studied for the oxidative cross-coupling between methanol and unsaturated alcohols (such as methallyl alcohol or allyl alcohol) on oxygen-activated Au(110) surface to give the corresponding methacrylate derivatives.[185] Authors evidenced that the presence of C=C bond increases the binding efficiency and the methyl group triggers an additional van der Waals interaction at the metal surface.

N-doped CoNPs (2.55 nm) supported on active carbon were applied to cross-couplings between substituted benzaldehydes and methanol under oxygen flow.[186] CoNPs were prepared by pyrolysis under N_2, from $Co(NO_3)_2$ adsorbed on active carbon with a melamine-formaldehyde resin, followed by H_2SO_4 treatment. XPS analyses evidenced a Co-*N*-pyridine interaction based on the positive shift of the N1s binding energy in relation to the metal-free support (398.1 eV *vs* 398.9 eV, respectively). Therefore, authors suggested that the activation of oxygen was promoted by the Co-*N* coordination sites; the pyridinic nitrogen atoms act as base promoting the deprotonation of methanol. Kinetic studies showed that the presence of hindered substituents on the aldehyde in *ortho*-position affects the reaction rate more than electronic effects, proving that the nucleophilic attack of the methoxy group to the carbonyl is the rate limiting step.

Shimizu and coworkers reported the synthesis of amides through hydration of nitriles, catalyzed by PdNPs@carbon.[187] The catalytic material (PdNPs exhibiting a mean size of 6.5 nm) was prepared by exposure of commercial Pd/C under H_2 at 500 °C followed by cooling to room temperature under He atmosphere. PXRD and EXAFS analyses showed that PdNPs were constituted of Pd(0). However, XPS analysis revealed also the presence of Pd(II) species at the surface of PdNPs. This as-prepared catalytic material was used for the hydration of nitriles in water. The presence of adsorbed oxygen atoms (acting as Bronsted base for the dissociation of water *via* hydrogen bond) and Pd(0) sites (acting as Lewis acid activating the nitrile moiety) led to a high catalytic activity (Fig. 26). The carbon-based support also showed a better adsorption ability in comparison to inorganic oxides (such as alumina or zircona) of methylacetates due to its higher hydrophobic nature. The kinetic isotope effect (KIE) of the acetonitrile hydration in H_2O and D_2O was relatively low (KIE = 1.2), indicating that the dissociation of water has an influence on the reaction rate but is not the determining step. The Hammet parameter was determined for *para*-substituted benzonitriles; the positive slope value indicated a negative charged transition

state for the rate determining step corresponding to the nucleophilic addition of OH^- species to the carbon of the nitrile group. DTF studies corroborated these experimental data.

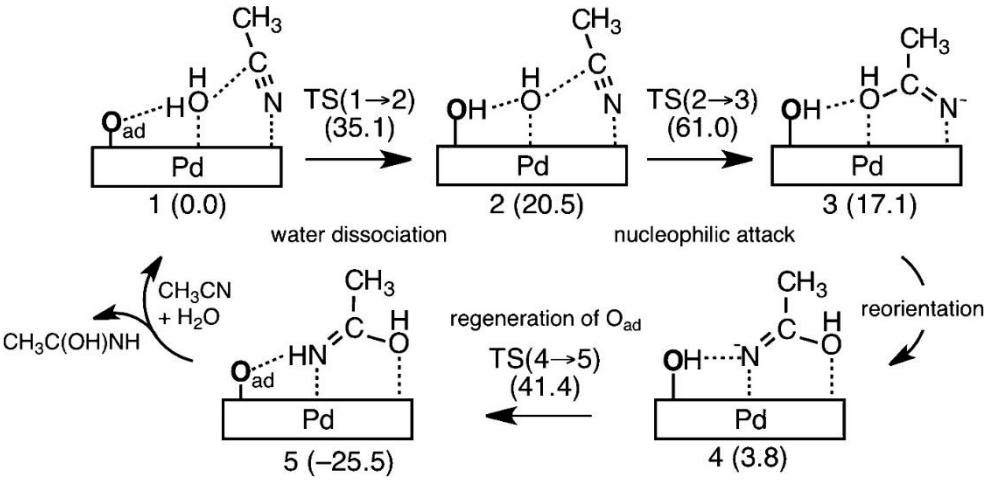

Fig. 26 Reaction mechanism hydration of acetonitrile (computed relative energies in kJ mol^{-1}) on the Pd(111) surface covered with the surface oxygen atom. Reprinted with permission from [187]. Copyright 2012 American Chemical Society

Ullmann-type couplings between haloarenes and phenol derivatives catalyzed by bimetallic spinel-nano-materials, in particular M-based ferrites (MFe_2O_4, where M = Cu,[188] Ni,[189,190], Co[190]), were highly active and selective towards the formation of aromatic ethers, being recyclable catalytic systems. Control tests evidenced that the coupling process proceeded through oxidative addition of the haloarene facilitated by the high surface of NPs and their easier electron transfer, discarding a nucleophilic substitution; furthermore, these couplings were not promoted by radical intermediates. A synergetic effect between M and iron in these ferrites seems likely by electronic transfer between M(II) and Fe(III).

Decarboxylation processes of fatty acids to give long-chain alkenes or alkanes exhibit a great interest to substitute non-renewable fossil fuel resources.[191,192] Both experimental and theoretical studies on carboxylic acids indicate that the decarboxylation occurs through an initial activation and dehydrogenation of C-H bonds in 2 and 3 positions (related to COOH function) before producing the C-O or C-C bond scission. In particular, AuNPs have proven their efficiency in many oxidation reactions.[193-195] From a mechanistic point of view, Yates and coworkers studied the oxidative dehydrogenation of acetic, propionic and butyric acids promoted by AuNPs (*ca.* 3 nm) supported on TiO_2 to form $Au_2C=C=O$ ketenylidene species (Fig. 27).[196] *In-situ* FT-IR analysis confirmed that carboxylates were adsorbed on TiO_2 surface after deprotonation of the COOH function. Then O_2 dissociates at the dual Au-Ti(IV) sites giving O ad atoms on Au surface, which act as Lewis base for the further C-H bond activation. FT-IR analysis also proved the formation of $Au_2C=C=O$. Experiments run under $^{18}O_2$ (no $Au_2C=C=^{18}O$ species was observed) or under vacuum (no formation of $Au_2C=C=O$ in the absence of oxygen) indicate that gold ketenylidene species are formed firstly by activation of the C-H bonds followed by the C-O bond activation. The absence of kinetic isotopic effects with deuterated propionic and butyric acids reveals that the C-H bond cleavage is not the rate determining step and that the dehydrogenation step occurs before the C-O (rate determining step) and the C-C bond cleavage.

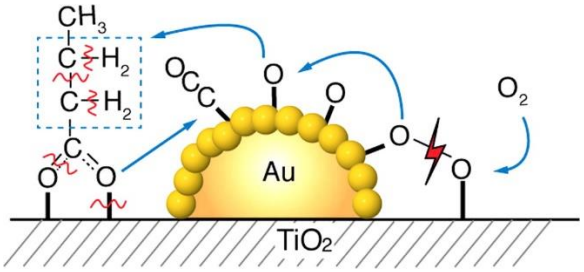

Fig. 27 Partial oxidation of acetic, propionic, and butyric carboxylic acids on Au/TiO_2 catalysts. Reprinted with permission from [196]. Copyright 2014 American Chemical Society

4.2. C-N bond formation reactions

Che and coworkers applied AuNPs (*ca*. 14.5 nm) supported on graphite in the oxidation of different organic compounds under oxygen, in particular the formation of *N*-(benzylidene)benzylamines benzylamines from benzylamines.[197] In contrast to Ru-based catalysts which preferentially lead to the formation of nitriles,[198] AuNPs@graphite gave selectively *N*-(benzylidene)benzylamines. Based on several studies, such as radical trap tests, Hammet plot and kinetics experiments, authors proposed a mechanism including a hydrogen-transfer process from the benzylamine to the metal and an oxidation step involving metal hydrides at the AuNPs surface (Fig. 28).

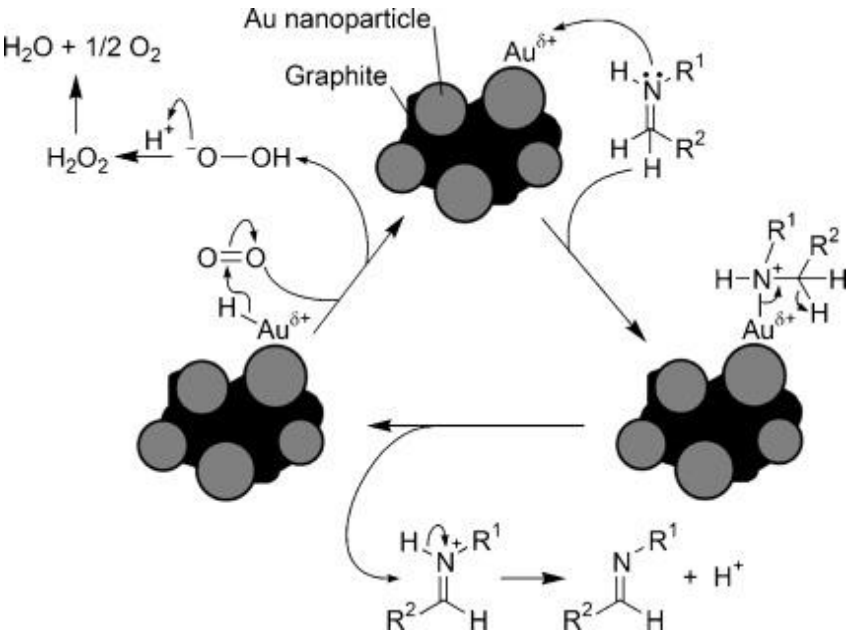

Fig. 28 Mechanism of Aerobic Oxidation of Benzylic Amines to Imines involving AuNPs@graphite as catalyst. Reprinted from [197]. Copyright 2009 Wiley-VCH Verlag GmbH & Co. KGaA, Weinheim

Thus, the first step corresponds to the amine coordination at $Au^{\delta+}$ surface sites. The participation of positively-charged intermediates was inferred from the negative slope of the Hammett plot (ρ parameter) for the oxidation of para-substituted benzylamines. Then, C-H bond cleavage takes place at the benzylic position, being the rate determining step deduced from kinetic isotopic effects. A β-hydride shift occurs at the AuNPs surface and then O_2 acts as an H acceptor giving H_2O_2 (not detected due to the high temperature of the reaction, 110 °C). This role of H-acceptor of oxygen was confirmed by the control reaction (oxidation of dibenzylamine to *N*-(benzylidene)benzylamine in presence of H_2O_2 under Ar atmosphere, but exhibiting a lower yield). The presence 2,6-di-*tert*-butyl-4-methylphenol as radical scavenger did not perturb the reaction.

Beller and coworkers described the synthesis of sulfonamides catalyzed by RuNPs supported on magnetic Fe_3O_4, through an eco-friendly approach consisting of direct coupling between unfunctionalized sulfonamides and alcohols.[199] A dehydrogenation-condensation-hydrogenation tandem process took place. Kinetic isotopic effect was observed for the competitive reactions of benzylic alcohol-d_7 and benzylic alcohol with *p*-toluensulfonamide, indicating that the alcohol dehydrogenation was the rate determining step (k_H/k_D = 2.86 for the benzyl alcohol dehydrogenation and k_H/k_D = 0.74 for the hydrogenation of *N*-benzylidene-*p*-toluenesulfonamide) (Scheme 1).

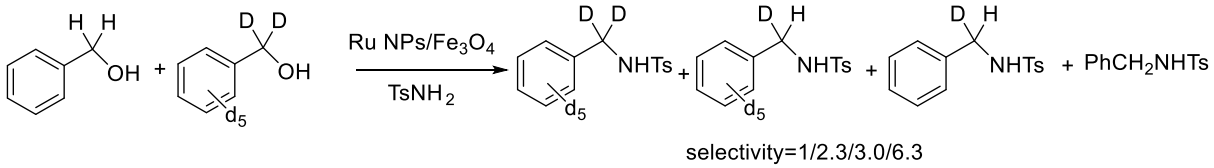

Scheme 1 dehydrogenation-condensation-hydrogenation tandem process catalyzed by RuNPs supported on magnetic Fe_3O_4.

Garcia and coworkers reported iron and cobalt based nanocatalysts, supported on a graphitic carbon matrix, including FeCo alloys (sizes in the range 10.9 – 26.5 nm), to be applied in C-N oxidative coupling of aromatic N-H and amide compounds.[200] FeNPs@C (mainly constituted of Fe(0) (XRD analysis) with the presence of Fe(II) and Fe(III) at the metallic surface proven by XPS) appeared as the most active and recyclable system, for which some mechanistic insights were carried out, mainly focused on the characterization of the organic intermediates. These studies showed that the amide radical is the key intermediate of the process, while FeNPs are the responsible to form the first radicals by TBHP degradation (Fig. 29).

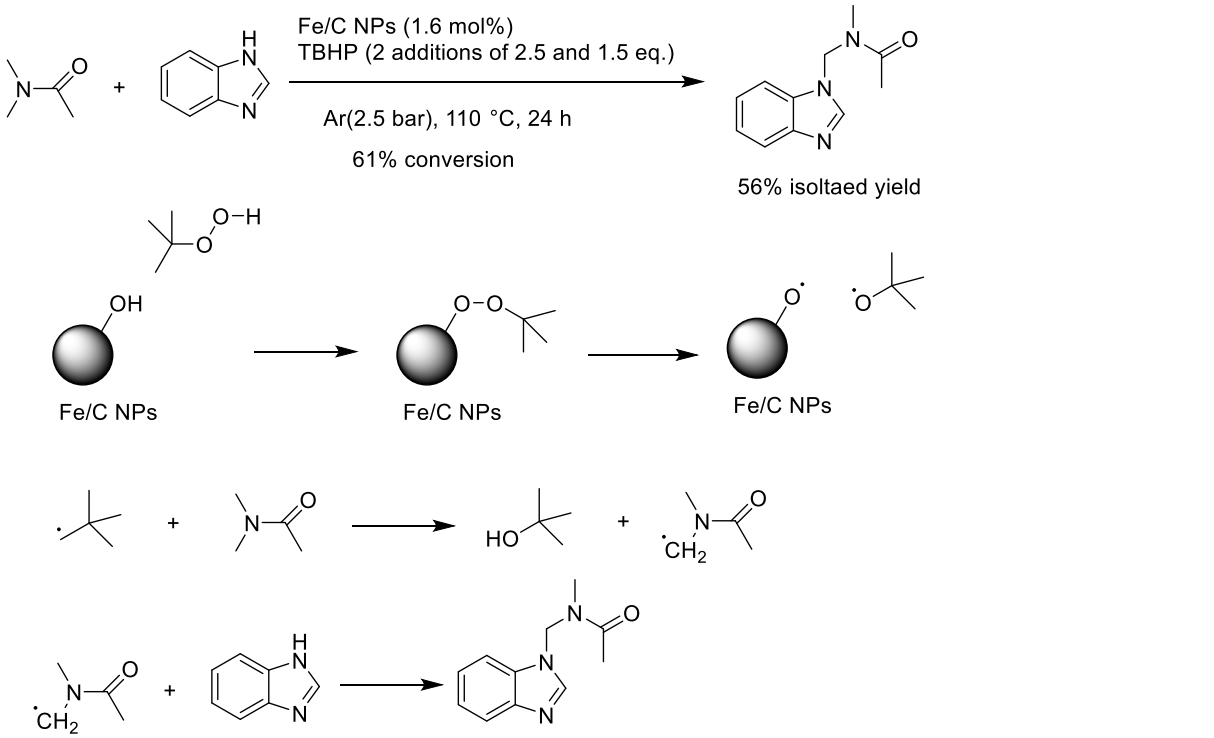

Fig. 29. C-N oxidative coupling of aromatic N-H and amide compounds catalyzed by FeNPs@C.

4.3. A^3 coupling

Three components tandem reaction of Aldehyde, Alkyne and Amine, commonly called A^3 coupling, has received a lot of attention in recent years.[201-203] Indeed, it leads to the synthesis of propargylamines and their derivatives, useful precursors in the development of different organic substrates, natural products, and drugs.[204]

Over the last decades, different catalytic systems have been investigated for convenient preparation of propargylamines under green conditions. Thus, homogeneous catalytic systems based on transition-metal salts have been reported, presenting high reactivity and selectivity.[201] In the heterogeneous catalyzed methodology, a large number of A^3 couplings catalyzed by MNPs (*e.g.* Cu, Au, Ag, Ni, Fe, Co and Zn) have been reported, however the research of their catalytic mechanism remains limited.[205,206] Generally, mechanisms based on the formation of well-known π complexes between metals and alkynes (R–C≡C–M) are proposed, which then react with the iminium ion formed by condensantion between the aldehyde and the amine, resulting in the production of the corresponding propargylamine and regeneration of the metal catalyst. However, when CuNPs synthesized in glycerol were used, the mechanism appeared to be different, as evidenced by spectroscopic means (Fig. 30).[207] Actually, FT-IR studies proved a weak $\sigma-\pi$ bonding interaction between phenylacetylene and the metal surface [broad band showing a $\Delta\nu \sim$ -30 cm^{-1} in relation to free phenylacetylene: 2108 (free Ph-C≡C-Ph) *vs* 2070 (capping Ph-C≡C-Ph) cm^{-1}; for phenylethynylcopper(I), the C≡C stretching appeared as a narrow absorption band at 1927 cm^{-1}), in accordance with that observed for RuNPs.[208] Moreover, UV-vis analyses showed that the surface plasmon resonance absorption band of CuNPs was not affected by the presence of phenylacetylene (578 nm), being larger most likely due to the capping effect triggerend by the absoprption of reagents at the metal surfaced; after addition of morpholine, an extra absorption band appeared, attributed to a M-L charge transfer transition. This behavior is in clear contrast with that observed with phenylethynylcopper(I) where two absorption bands were observed due to a M-L charge transfer band and an intramolecular $\pi-\pi^*$ ligand band; in the presence of morpholine, free phenylacetylene was released and Cu(II) species were formed. These spectroscopic data point out a surface-like reactivity, proving the absence of molecular copper species.

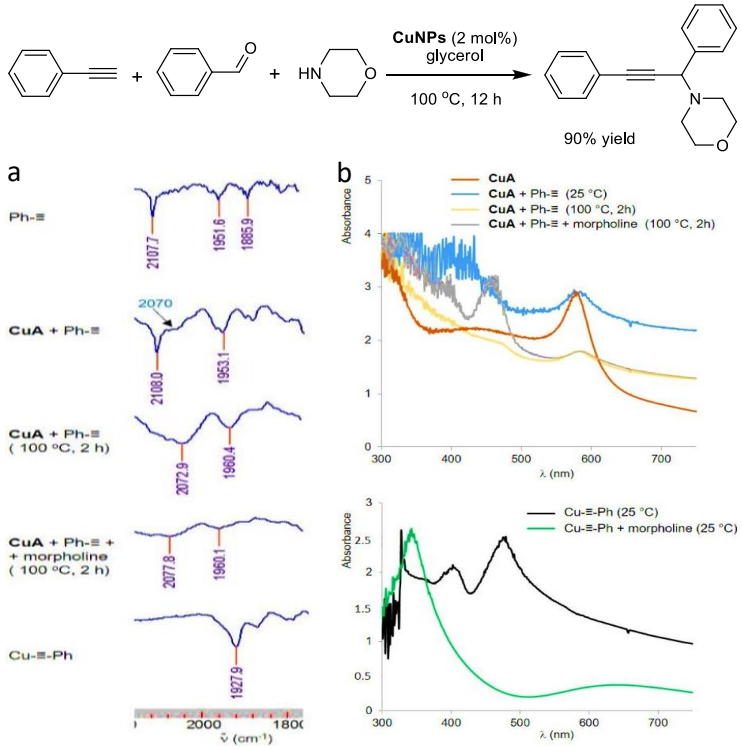

Fig. 30 (Top) Synthesis of propargylamine catalyzed by CuNPs in glycerol. (Bottom) FT-IR (a) and UV-vis (b) spectra corresponding to the experiments of CuNPs, phenylacetylene and morpholine in glycerol. Reproduced from [207]. Copyright 2017 Wiley-VCH Verlag GmbH & Co. KGaA, Weinheim.

4.4. Oxyhalogenation reactions

Catalytic methane oxyhalogenation is the process involving the C-H bond activation of methane with hydrogen halide and oxygen, leading to the generation of hydroalkanes and water. It permits the methane functionalization with HX recovery.[209,210] This methodology appears particularly interesting for the selective transformation of methane and light hydrocarbons (C2-C4), which represents an important current challenge. Ideally, the catalyst must simultaneously activate the three reagents, precluding alkyl halide oxidation and further halogenation. Pérez-Ramirez and co-workers have recently reported the methane oxychlorination and oxybromination catalyzed by noble nanoparticles supported on SiO_2 (mean diameter of MNPs in the range of 6-18 nm), such as Ru-, Pt-, Ir-, Rh- and Pd-based NPs, being RuO_2 NPs the most active catalytic system (Fig. 31).[211] Authors evidenced the transformation of the metal oxide nanoparticles into metal silicide, metal, and halogenated phases during the reaction (PXRD and Raman analyses), proving the high reactivity shown by the catalyst surfaces. Operando photoelectron photoion coincidence spectroscopy (PEPICO) analyses carried out over Pd-based NPs@SiO_2, proved that the catalyst promotes the formation of radical halide species, which are the responsible of the methane activation in the gas phase; activation at the catalyst surface cannot be ruled out.

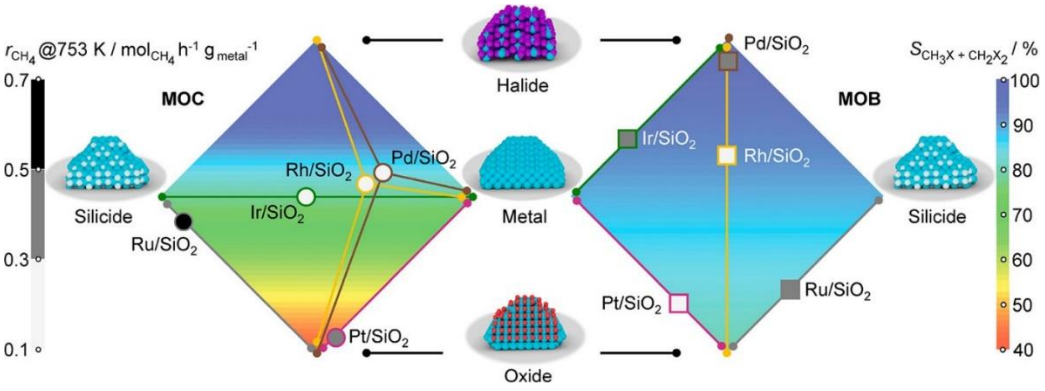

Fig. 31 SiO_2-supported catalysts structure−performance relationships for methane oxychlorination (MOC left) and oxybromination (MOB right). The left scale indicates catalyst reactivity: low (light gray), medium (gray), high (black) for methane oxyhalogenation at 753 K. The right scale indicates the total selectivity to halomethanes at 753 K and at ca. 20% methane conversion, corresponding to the mark on diamond map. The lines arising from the symbols point to the phases identified by X-ray diffraction and Raman analysis which vary from metal halides (top), to metallic (center), metal silicides (left and right), and metal oxides (bottom). Reprinted with permission from [211]. Copyright 2019 American Chemical Society

5. Fischer-Tropsch reaction

Fischer-Tropsch reaction (FT) is a process which converts syngas, a mixture of H_2 and CO, into hydrocarbons mainly for fuel applications but also for the synthesis of valuable chemicals.[212-214] Fe, Co, Ni and Ru based NPs are commonly applied for this transformation.

Regarding FT mechanism, it is accepted that the process follows a step-wise carbon chain growth, after an initial activation of both H_2 and CO at the metal surface of the nanocatalyst. Numerous research groups studied the chain growth processes. In the scope of this review, the interaction between reactants and MNPs surface is highlighted.

The reaction mechanism for FT synthesis with iron catalysts has been reported by B. Devis.[215] One of the difficulties to study this mechanism is related to the ability of metals to transform into their corresponding oxides or carbides. The role of carbides and their performance in FT is still not totally clear and represent a goal of current studies.[216,217] In 2016, Chaudret and coworkers proposed an elegant approach using labelled ^{13}CO to monitor the reaction by gas-phase NMR spectroscopy and mass spectrometry.[218] It was demonstrated that iron carbide NPs can be labeled with ^{13}C to study their

role in the CO hydrogenation. Heating of the as-prepared nanomaterial at 250 °C under H_2 led to the carbon desorption and exclusive formation of methane. When the reaction was performed at 210 °C, a mixture of unlabeled hydrocarbons was observed, suggesting the absence of exchange between carbide C atoms at the metal surface and CO in the gas phase. Contrarily, the presence of $^{13}CH_4$ was demonstrated at 250 °C, confirming that FT process goes through a surface carbide mechanism (Fig. 32).

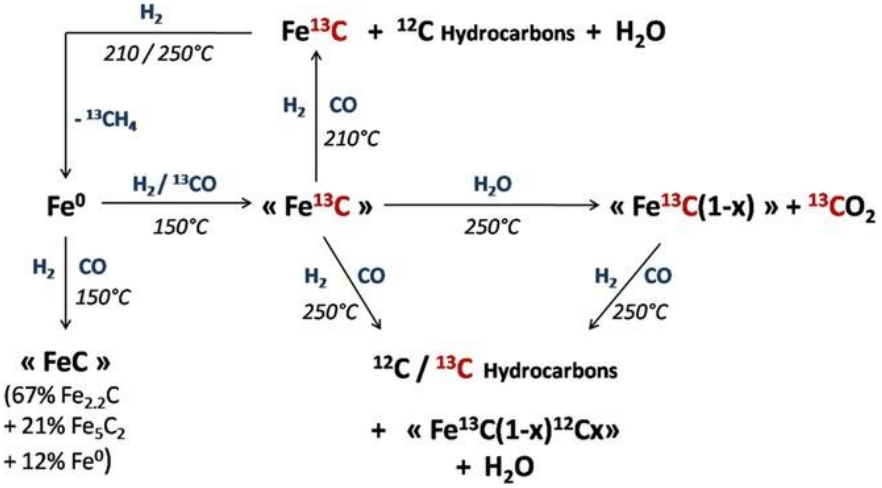

Fig. 32 Reactions investigated for iron carbide NPs. Reproduced from [218]. Copyright 2016 Wiley-VCH Verlag GmbH & Co. KGaA, Weinheim.

These observations are in agreement with computational works proving the formation of $CH_X(O)$ and C_1 products (CH_4, CH_2O, and CH_3OH) from iron carbide surface with different carbon content.[219]
DFT calculations have also been used to investigate the FT reaction mechanism for oxide-modified nickel catalysts (NiO_X/Ni).[220] The authors compared the potential-energy profiles for syngas conversion on NiNPs and NiO_X/Ni, as well as for C-C coupling reactions. It was proposed that the production of hydrocarbons was favored on the NiO_X/Ni surface, in agreement with experimental data.
Regarding CoNPs, Weststrate *et al*. proposed a chain growth mechanism, in which CO is adsorbed on the NPs surface and alkylidyne reacts as the chain initiator.[221] Their investigations were based on experimental techniques, such as IR spectroscopy (Fig. 33), as well as DFT calculations.

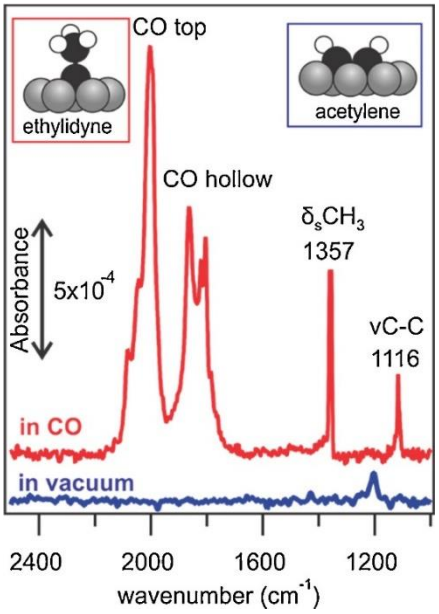

Fig. 33 FT-IR spectra of an adsorbed acetylene + 2 H layer on CoNPs at 250 K in vacuum (blue) and in the presence of 1×10^{-6} mbar CO (red). Reprinted from [221] with permission from Elsevier.

The same group also performed synchrotron-based high-resolution XPS to determine both the nature and concentration of the C_xH_y surface intermediates on *fcc*-CoNPs surface.[221] The experiments showed that CO promotes the transformation of C_2H_x adsorbates into ethylidyne and its further dimerization (Fig. 34)

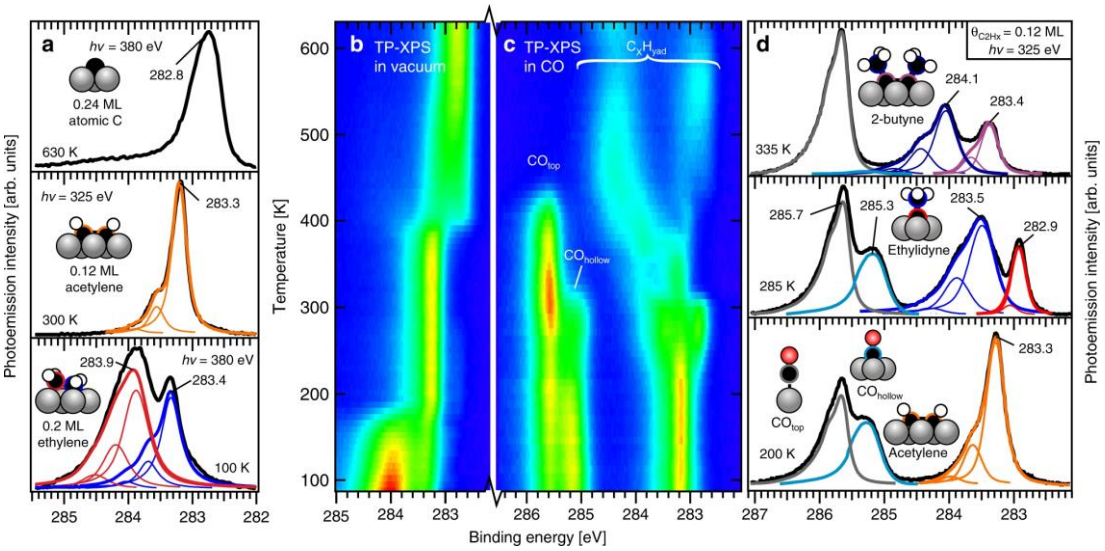

Fig. 34 (a) High resolution XPS spectra after heating ethylene-saturated Co(0001)NPs under vacuum conditions at the indicated temperatures; (b) Heat map of C1s XPS spectra carried out during the heating of ethylene-covered CoNPs under vacuum conditions; (c) Heat map of C1s XPS spectra carried out during the heating of $C_2H_{2ad}/2H_{ad}$-covered surface in the presence of CO (1×10^{-7} mbar); (d) High resolution XPS spectra after heating $C_2H_{2ad}/2H_{ad}$ in CO at the indicated temperatures. *Note: for b and c, h ν = 380 eV at 7 K for each spectrum; blue means low intensity; red, high intensity (heating rate of 0.2K s^{-1})*. Reprinted from [222] with permission from Springer Nature.

Martínez and coworkers investigated the influence of Ru concentration in bimetallic CoRuNPs@TiO_2 (10 wt% of Co and 0.1-1.2 wt% of Ru) on FT synthesis.[223] The FT activity in terms of metal-time-yield and initial turnover frequency was analyzed for both Ru-free and Ru-doped catalytic materials. It was observed that both catalytic parameters were maximized for catalysts with 0.1–0.2 wt% Ru. To understand this behavior, *in situ* characterizations were performed. FT-IR experiments under flowing syngas at 220 °C and 1 bar showed the CoNPs surface reconstruction, creating more defected Co(0) with the highest Ru content (1.2 wt % of Ru). Unfortunately, the lack of surface reconstruction was observed for Ru free Co@TiO_2 system, for which linear CO-Co^0 IR vibration band stays unchanged at 220 °C. Thus, the lower amount of Co(0) sites in Co@TiO_2 system could be at the origin of its lower FT activity in comparison to CoRu@TiO_2. Furthermore, *in situ* XPS analysis revealed that the CoNPs surface remained zero-valent during FT reaction when it was catalyzed by CoRu@TiO_2 with low Ru loading (0.1-0.2 wt%), while oxide-like cobalt nanoparticles (CoO_X) were detected for samples with Ru content higher than 0.2 wt%. Such effect could arise from a partial electron charge transfer from Co(0) to the more electronegative Ru(0), favoring the adsorption of O atoms formed upon CO dissociation on positively charged $Co^{\delta+}$ at high Ru content (Fig. 35). In the absence of Ru, Auger spectrum of Co@TiO_2 showed the shoulder at 779.5 eV which was attributed to the formation of cobalt carbide species during the FT reaction.

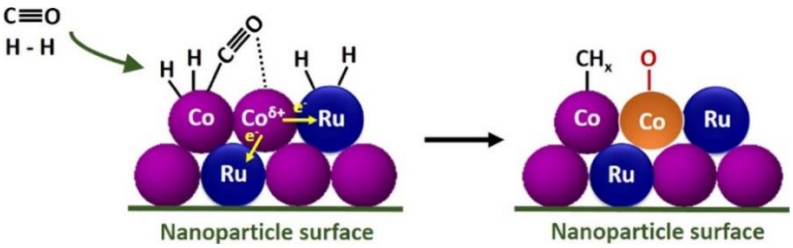

Fig. 35 Schematic representation of the formation of Co−O species on positively charged surface Co atoms in CoRu@TiO_2 with Ru content was higher than 0.2 wt%. Reprinted with permission from [223]. Copyright 2020 American Chemical Society.

Based on these experimental results, authors concluded that the FT activity for CoRu@TiO_2 catalytic materials is limited by the formation of CoC_X (in the absence of Ru promoter) and the presence of CoO_X (at Ru loading above 0.2 wt%) (Fig. 36).

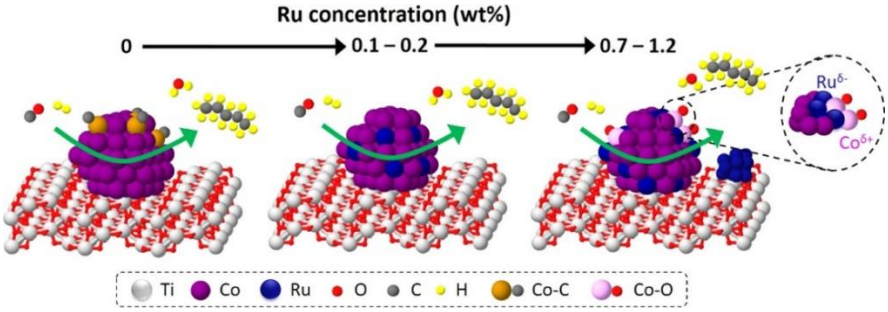

Fig. 36 Schematic representation of the influence of Ru content on the nature of surface cobalt species in Co-Ru@TiO_2 under FT conditions, showing the formation of Co−C in the absence of Ru and of Co−O at high Ru concentration >0.2 wt %. Reprinted with permission from [223]. Copyright 2020 American Chemical Society.

6. Conclusions and perspectives

This review focused on coupling reactions catalyzed by preformed (un)supported metal-based nanoparticles, including mechanistic studies in particular those that highlight substrate-metal interactions at the surface of the nanocatalysts. These transformations often work under complex conditions, involving several reagents, solvents and/or additives, making mechanistic studies difficult both at experimental and computational level. Design of appropriate experiments together with analysis by cutting-edge techniques permit to evidence specific metal-reagent interactions at the surface of nanoparticles.

The surface activation pathways via synergistic effects between nanoparticles and supports, taking into account reaction kinetics are key to the development of orthogonal transformations. Thus far, Glaser-Hay heterocouplings for the preparation of unsymmetrical 1,3-diynes has been achieved with nanocatalyst composites of small Cu/Cu_2O NPs on covalent organic frameworks.[224] In addition, the exploitation of novel activation modes by means of surface plasmon resonance effects, magnetic properties, and light harvesting capabilities, among others, brings forth new opportunities for tailor-made catalytic nanomaterials. From a mechanistic point of view, the advances on characterization tools, including operando techniques in order to allow reaction monitoring, signify a major challenge in this field.

Acknowledgments

The Centre National de la Recherche Scientifique (CNRS) and the Université Toulouse 3 – Paul Sabatier are gratefully acknowledged for their financial support. Authors thank to POCTEFA Interreg program for funding this work (EFA308/19 TRIPyr).

REFERENCES

1. Schmid G. *Nanoparticles: From Theory to Application*. Wiley-VCH Verlag; 2011.

2. Serp P, Philippot K. *Nanomaterials in Catalysis*. Wiley-VCH Verlag GmbH; 2013:I-XX.
3. Martínez-Prieto LM, Chaudret B. Organometallic Ruthenium Nanoparticles: Synthesis, Surface Chemistry, and Insights into Ligand Coordination. *Acc Chem Res*. 2018;51:376-384.
4. Adil SF, Assal ME, Khan M, Al-Warthan A, Siddiqui MRH, Liz-Marzán LM. Biogenic Synthesis of Metallic Nanoparticles and Prospects Toward Green Chemistry. *Dalton Trans*. 2015;44:9709-9717.
5. Ghosh Chaudhuri R, Paria S. Core/Shell Nanoparticles: Classes, Properties, Synthesis Mechanisms, Characterization, and Applications. *Chem Rev*. 2012;112:2373-2433.
6. Zhou B, Hermans S, Somorjai GA. *Nanotechnology in Catalysis*. Kluwer Academics/Plenum; 2004.
7. An K, Alayoglu S, Ewers T, Somorjai GA. Colloid chemistry of nanocatalysts: A molecular view. *J Colloid Interface Sci*. 2012;373:1-13.
8. Corain B, Schmid G, Toshima N. *Metal Nanoclusters in Catalysis and Materials Science: The Issue of Size Control*. Elsevier Science; 2011.
9. Astruc D. *Nanoparticles and Catalysis*. Wiley-VCH Verlag GmbH; 2008:I-XXIII.
10. Heiz U, Landman U. *Nanocatalysis*. Springer 2007.
11. Torimoto T, Kameyana T, Kuwabata S. Top-down Synthesis Methods for Nanoscale Catalysts. In: Prechtl MHG, ed. *Nanocatalysis in Ionic Liquids*. Wiley-VCH; 2017, pp 171-205:chap 9.
12. Roucoux A, Schulz J, Patin H. Reduced Transition Metal Colloids: a Novel Family of Reusable Catalysts? *Chem Rev*. 2002;102:3757-3778.
13. Burda C, Chen X, Narayanan R, El-Sayed MA. Chemistry and Properties of Nanocrystals of Different Shapes. *Chem Rev*. 2005;105:1025-1102.
14. Amiens C, Chaudret B, Ciuculescu-Pradines D, et al. Organometallic approach for the synthesis of nanostructures. *New J Chem*. 2013;37:3374-3401.
15. Xi G, Peng Y, Yu W, Qian Y. Synthesis, Characterization, and Growth Mechanism of Tellurium Nanotubes. *Cryst Growth Des*. 2005;5:325-328.
16. Mitsutaka O, Susumu T, Masakazu I, Masatake H. Chemical Vapor Deposition of Gold Nanoparticles on MCM-41 and Their Catalytic Activities for the Low-temperature Oxidation of CO and of H_2. *Chem Lett*. 1998;27:315-316.
17. Reina A, Jia XT, Ho J, Nezich D, Son HB, Bulovic V, Dresselhaus MS, Kong J. Large area, few layer graphene films on arbitrary substrates by chemical vapor deposition. *Nano Lett*. 2009;9:30-35.
18. Sivula K, Formal FL, Grätzel M. WO3−Fe2O3 Photoanodes for Water Splitting: A Host Scaffold, Guest Absorber Approach. *Chem Mater*. 2009;21:2862-2867.
19. Gelesky MA, Umpierre AP, Machado G, Correia RRB, Magno WC, Morais J, Ebeling G, Dupont J. Laser-Induced Fragmentation of Transition Metal Nanoparticles in Ionic Liquids. *J Am Chem Soc*. 2005;127:4588-4589.
20. Dai ZR, Pan ZW, Wang ZL. Novel Nanostructures of Functional Oxides Synthesized by Thermal Evaporation. *Adv Funct Mater*. 2003;13:9-24.
21. Wasa K, Kitabatake M, Adachi H. *Thin film materials technology: sputtering of control compound materials*. Springer-Verlag 2004.
22. Dang-Bao T, Favier I, Gómez M. Metal Nanoparticles in Polyols: Bottom-up and Top-down Syntheses and Catalytic Applications. In: Philippot K, Roucoux A, eds. *Nanoparticles in Catalysis*. Wiley Professional, Reference & Trade (Wiley K&L); 2021, pp 99-122.
23. Wender H, de Oliveira LF, Migowski P, Feil AF, Lissner E, Prechtl MHG, Teixeira SR, Dupont J. Ionic Liquid Surface Composition Controls the Size of Gold Nanoparticles Prepared by Sputtering Deposition. *J Phys Chem C*. 2010;114:11764-11768.
24. Torimoto T, Okazaki K-i, Kiyama T, Hirahara K, Tanaka N, Kuwabata S. Sputter deposition onto ionic liquids: Simple and clean synthesis of highly dispersed ultrafine metal nanoparticles. *Appl Phys Lett*. 2006;89:243117.
25. Wender H, Migowski P, Feil AF, Teixeira SR, Dupont J. Sputtering deposition of nanoparticles onto liquid substrates: Recent advances and future trends. *Coord Chem Rev*. 2013;257:2468-2483.
26. Wang J, Gu H. Novel Metal Nanomaterials and Their Catalytic Applications. *Molecules*. 2015;20:17070-17092.

27. Alshammari A, Kalevaru VN, Martin A. Metal Nanoparticles as Emerging Green Catalysts. In: Larramendy M, Soloneski S, eds. *Green Nanotechnology: Overview and Further Prospects*. IntechOpen; 2016.
28. Khalil M, Kadja GTM, Ilmi MM. Advanced nanomaterials for catalysis: Current progress in fine chemical synthesis, hydrocarbon processing, and renewable energy. *J Ind Eng Chem*. 2021;93:78-100.
29. Durand J, Teuma E, Gómez M. An Overview of Palladium Nanocatalysts: Surface and Molecular Reactivity. *Eur J Inorg Chem*. 2008;2008:3577-3586.
30. de Vries JG. A unifying mechanism for all high-temperature Heck reactions. The role of palladium colloids and anionic species. *Dalton Trans*. 2006:421-429.
31. Phan NTS, Van Der Sluys M, Jones CW. On the Nature of the Active Species in Palladium Catalyzed Mizoroki–Heck and Suzuki–Miyaura Couplings – Homogeneous or Heterogeneous Catalysis, A Critical Review. *Adv Synth Catal*. 2006;348:609-679.
32. Vasconcelos SNS, Reis JS, de Oliveira IM, Balfour MN, Stefani HA. Synthesis of symmetrical biaryl compounds by homocoupling reaction. *Tetrahedron*. 2019;75:1865-1959.
33. Ullmann F, Bielecki J. Ueber Synthesen in der Biphenylreihe. *Ber Dtsch Chem Ges*. 1901;34:2174-2185.
34. Goldberg I. Ueber Phenylirungen bei Gegenwart von Kupfer als Katalysator. *Ber Dtsch Chem Ges*. 1906;39:1691-1692.
35. Monnier F, Taillefer M. Catalytic C-C, C-N, and C-O Ullmann-Type Coupling Reactions. *Angew Chem, Int Ed*. 2009;48:6954-6971.
36. Sambiagio C, Marsden SP, Blacker AJ, McGowan PC. Copper catalysed Ullmann type chemistry: from mechanistic aspects to modern development. *Chem Soc Rev*. 2014;43:3525-3550.
37. Ribas X, Gueell I. Cu(I)/Cu(III) catalytic cycle involved in Ullmann-type cross-coupling reactions. *Pure Appl Chem*. 2014;86:345-360.
38. Beletskaya IP, Cheprakov AV. Copper in cross-coupling reactions: The post-Ullmann chemistry. *Coord Chem Rev*. 2004;248:2337-2364.
39. Hassan J, Sevignon M, Gozzi C, Schulz E, Lemaire M. Aryl-aryl bond formation one century after the discovery of the Ullmann reaction. *Chem Rev*. 2002;102:1359-1469.
40. Lewis EA, Murphy CJ, Liriano ML, Sykes ECH. Atomic-scale insight into the formation, mobility and reaction of Ullmann coupling intermediates. *Chem Commun*. 2014;50:1006-1008.
41. Lewis EA, Murphy CJ, Pronschinske A, Liriano ML, Sykes ECH. Nanoscale insight into C-C coupling on cobalt nanoparticles. *Chem Commun*. 2014;50:10035-10037.
42. Wang W, Chen S, Guisasola Cal E, Martinez Moro M, Moya S, Coy E, Wang C, Hamon J-R, Astruc D. ZIF-8-based vs. ZIF-8-derived Au and Pd nanoparticles as efficient catalysts for the Ullmann homocoupling reaction. *Inorg Chem Front*. 2020;7:3945-3952.
43. Lanterna AE, Elhage A, Scaiano JC. Heterogeneous photocatalytic C-C coupling: mechanism of plasmon-mediated reductive dimerization of benzyl bromides by supported gold nanoparticles. *Catal Sci Technol*. 2015;5:4336-4340.
44. Crabbe BW, Kuehm OP, Bennett JC, Hallett-Tapley GL. Light-activated Ullmann homocoupling of aryl halides catalyzed using gold nanoparticle-functionalized potassium niobium oxides. *Catal Sci Technol*. 2018;8:4907-4915.
45. Zhang S, Li J, Gao W, Qu Y. Insights into the effects of surface properties of oxides on the catalytic activity of Pd for C-C coupling reactions. *Nanoscale*. 2015;7:3016-3021.
46. Chumkaeo P, Poonsawat T, Meechai T, Somsook E. Synergistic Activities in the Ullmann Coupling of Chloroarenes at Ambient Temperature by Pd-Supported Calcined Ferrocenated La_2O_3. *Appl Organomet Chem*. 2019;33:n/a.
47. Varadwaj GBB, Rana S, Parida K. Pd(0) Nanoparticles Supported Organofunctionalized Clay Driving C-C Coupling Reactions under Benign Conditions through a Pd(0)/Pd(II) Redox Interplay. *J Phys Chem C*. 2014;118:1640-1651.
48. Tyagi A, Yamamoto A, Yoshida H. Photocatalytic Ullmann coupling of aryl halides by a novel blended catalyst consisting of a TiO_2 photocatalyst and an Al_2O_3 supported Pd-Au bimetallic catalyst. *Catal Sci Technol*. 2018;8:6196-6203.

49. Tyagi A, Yamamoto A, Yoshida H. Novel blended catalysts consisting of a TiO_2 photocatalyst and an Al_2O_3 supported Pd-Au bimetallic catalyst for direct dehydrogenative cross-coupling between arenes and tetrahydrofuran. *RSC Adv*. 2018;8:24021-24028.
50. Favier I, Toro M-L, Lecante P, Pla D, Gómez M. Palladium-mediated Radical Homocoupling Reactions: a Surface Catalytic Insight. *Catal Sci Technol*. 2018;8:4766-4773.
51. Dhital RN, Sakurai H. Oxidative Coupling of Organoboron Compounds. *Asian J Org Chem*. 2014;3:668-684.
52. Poupart R, Benlahoues A, Le Droumaguet B, Grande D. Porous Gold Nanoparticle-Decorated Nanoreactors Prepared from Smartly Designed Functional Polystyrene-block-Poly(D,L-Lactide) Diblock Copolymers: Toward Efficient Systems for Catalytic Cascade Reaction Processes. *ACS Appl Mater Interfaces*. 2017;9:31279-31290.
53. Blanco M, Mosconi D, Tubaro C, et al. Palladium nanoparticles supported on graphene acid: a stable and eco-friendly bifunctional C-C homo- and cross-coupling catalyst. *Green Chem*. 2019;21:5238-5247.
54. Prastaro A, Ceci P, Chiancone E, Boffi A, Fabrizi G, Cacchi S. Homocoupling of arylboronic acids and potassium aryltrifluoroborates catalyzed by protein-stabilized palladium nanoparticles under air in water. *Tetrahedron Lett*. 2010;51:2550-2552.
55. Carrettin S, Guzman J, Corma A. Supported Gold Catalyzes the Homocoupling of Phenylboronic Acid with High Conversion and Selectivity. *Angew Chem Int Ed*. 2005;44:2242-2245.
56. Tsunoyama H, Sakurai H, Ichikuni N, Negishi Y, Tsukuda T. Colloidal Gold Nanoparticles as Catalyst for Carbon-Carbon Bond Formation: Application to Aerobic Homocoupling of Phenylboronic Acid in Water. *Langmuir*. 2004;20:11293-11296.
57. Vijay A, Mills G, Metiu H. Adsorption of gold on stoichiometric and reduced rutile TiO_2 (110) surfaces. *J Chem Phys*. 2003;118:6536-6551.
58. Boronat M, Corma A. Molecular approaches to catalysis. *J Catal*. 2011;284:138-147.
59. Turner M, Golovko VB, Vaughan OPH, Abdulkin P, Berenguer-Murcia A, Tikhov MS, Johnson BFG, Lambert RM. Selective oxidation with dioxygen by gold nanoparticle catalysts derived from 55-atom clusters. *Nature*. 2008;454:981-983.
60. Liu Y, Tsunoyama H, Akita T, Xie S, Tsukuda T. Aerobic oxidation of cyclohexane catalyzed by size-controlled Au clusters on hydroxyapatite: size effect in the sub-2 nm regime. *ACS Catal*. 2011;1:2-6.
61. Shi W, Lei A. 1,3-Diyne chemistry. Synthesis and derivations. *Tetrahedron Lett*. 2014;55:2763-2772.
62. Liu J, Lam JWY, Tang BZ. Acetylenic Polymers: Syntheses, Structures, and Functions. *Chem Rev*. 2009;109:5799-5867.
63. Shun ALKS, Tykwinski RR. Synthesis of naturally occurring polyynes. *Angew Chem, Int Ed*. 2006;45:1034-1057.
64. Kivala M, Diederich F. Conjugation and optoelectronic properties of acetylenic scaffolds and charge-transfer chromophores. *Pure Appl Chem*. 2008;80:411-427.
65. Glaser C. Beiträge zur Kenntniss des Acetenylbenzols. *Ber Dtsch Chem Ges*. 1869;2:422-424.
66. Eglinton G, Galbraith AR. Macrocyclic acetylenic compounds. I. Cyclotetradeca-1,3-diyne and related compounds. *J Chem Soc*. 1959:889-896.
67. Akhtar R, Zahoor AF. Transition metal catalyzed Glaser and Glaser-Hay coupling reactions: Scope, classical/green methodologies and synthetic applications. *Synth Commun*. 2020;50:3337-3368.
68. Alonso F, Yus M. Heterogeneous Catalytic Homocoupling of Terminal Alkynes. *ACS Catal*. 2012;2:1441-1451.
69. Murugan K, Nainamalai D, Kanagaraj P, Nagappan SG, Palaniswamy S. Green-Synthesized Nickel Nanoparticles on Reduced Graphene Oxide as an Active and Selective Catalyst for Suzuki and Glaser-Hay Coupling Reactions. *Appl Organomet Chem*. 2020;34:e5778.
70. Boronat M, Laursen S, Leyva-Perez A, Oliver-Meseguer J, Combita D, Corma A. Partially oxidized gold nanoparticles: A catalytic base-free system for the aerobic homocoupling of alkynes. *J Catal*. 2014;315:6-14.

71. Vilhanova B, Vaclavik J, Artiglia L, Ranocchiari M, Togni A, van Bokhoven JA. Subnanometer Gold Clusters on Amino-Functionalized Silica: An Efficient Catalyst for the Synthesis of 1,3-Diynes by Oxidative Alkyne Coupling. *ACS Catal*. 2017;7:3414-3418.
72. Solomon EI, Chen P, Metz M, Lee S-K, Palmer AE. Oxygen binding, activation, and reduction to water by copper proteins. *Angew Chem Int Ed*. 2001;40:4570-4590.
73. Jin L, Tolentino DR, Melaimi M, Bertrand G. Isolation of bis(copper) key intermediates in Cu-catalyzed azide-alkyne "click reaction". *Sci Adv*. 2015;1:e1500304/1.
74. Rodríguez-Rodríguez M, Llanes P, Pradel C, Pericàs MA, Gómez M. Key Non-Metal Ingredients for Cu-catalyzed “Click” Reactions in Glycerol: Nanoparticles as Efficient Forwarders. *Chem Eur J*. 2016;22:18247-18253.
75. Liu L, Matsushita T, Concepcion P, Leyva-Perez A, Corma A. Facile Synthesis of Surface-Clean Monodispersed CuO_x Nanoparticles and Their Catalytic Properties for Oxidative Coupling of Alkynes. *ACS Catal*. 2016;6:2211-2221.
76. Lu W, Sun W, Tan X, Gao L, Zheng G. Stabilized Cu/Cu_2O nanoparticles on rGO as an efficient heterogeneous catalyst for Glaser homo-coupling. *Catal Commun*. 2019;125:98-102.
77. Zhang G, Yi H, Zhang G, et al. Direct Observation of Reduction of Cu(II) to Cu(I) by Terminal Alkynes. *J Am Chem Soc*. 2014;136:924-926.
78. Bai R, Zhang G, Yi H, et al. Cu(II)-Cu(I) Synergistic Cooperation to Lead the Alkyne C-H Activation. *J Am Chem Soc*. 2014;136:16760-16763.
79. Zhang Y-Q, Kepcija N, Kleinschrodt M, et al. Homo-coupling of terminal alkynes on a noble metal surface. *Nat Commun*. 2012;3:2291/1.
80. Zaccheria F, Scotti N, Ravasio N. The Role of Copper in the Upgrading of Bioalcohols. *ChemCatChem*. 2018;10:1526-1535.
81. Aitchison H, Wingad RL, Wass DF. Homogeneous Ethanol to Butanol Catalysis-Guerbet Renewed. *ACS Catal*. 2016;6:7125-7132.
82. Alonso DM, Bond JQ, Serrano-Ruiz JC, Dumesic JA. Production of liquid hydrocarbon transportation fuels by oligomerization of biomass-derived C9 alkenes. *Green Chem*. 2010;12:992-999.
83. Kozlowski JT, Davis RJ. Heterogeneous Catalysts for the Guerbet Coupling of Alcohols. *ACS Catal*. 2013;3:1588-1600.
84. Panchenko VN, Paukshtis EA, Murzin DY, Simakova IL. Solid Base Assisted n-Pentanol Coupling over VIII Group Metals: Elucidation of the Guerbet Reaction Mechanism by DRIFTS. *Ind Eng Chem Res*. 2017;56:13310-13321.
85. Cassar L. Synthesis of aryl- and vinyl-substituted acetylene derivatives by the use of nickel and palladium complexes. *J Organomet Chem*. 1975;93:253.
86. Dieck HA, Heck FR. Palladium catalyzed synthesis of aryl, heterocyclic, and vinylic acetylene derivatives. *J Organomet Chem*. 1975;93:259.
87. Sonogashira K, Tohda Y, Hagihara N. Convenient synthesis of acetylenes. Catalytic substitutions of acetylenic hydrogen with bromo alkenes, iodo arenes, and bromopyridines. *Tetrahedron Lett*. 1975:4467.
88. Chinchilla R, Najera C. The Sonogashira reaction: a booming methodology in synthetic organic chemistry. *Chem Rev*. 2007;107:874-922.
89. Dang-Bao T, Pradel C, Favier I, Gómez M. Bimetallic Nanocatalysts in Glycerol for Applications in Controlled Synthesis. A Structure–Reactivity Relationship Study. *ACS Appl Nano Mater*. 2019;2:1033-1044.
90. Olekszyszen DN, Albuquerque BL, Silva DdO, Tripodi GL, de Oliveira DC, Domingos JB. Core-shell PdCu bimetallic colloidal nanoparticles in Sonogashira cross-coupling reaction: mechanistic insights into the catalyst mode of action. *Nanoscale*. 2020;12:1171-1179.
91. Thathagar MB, Kooyman PJ, Boerleider R, Jansen E, Elsevier CJ, Rothenberg G. Palladium nanoclusters in Sonogashira cross-coupling: A true catalytic species? *Adv Synth Catal*. 2005;347:1965-1968.
92. Xu W, Sun H, Yu B, Zhang G, Zhang W, Gao Z. Sonogashira Couplings on the Surface of Montmorillonite-Supported Pd/Cu Nanoalloys. *ACS Appl Mater Interfaces*. 2014;6:20261-20268.

93. Sultana S, Mech SD, Hussain FL, Pahari P, Borah G, Gogoi PK. Green synthesis of graphene oxide (GO)-anchored Pd/Cu bimetallic nanoparticles using Ocimum sanctum as bio-reductant: an efficient heterogeneous catalyst for the Sonogashira cross-coupling reaction. *RSC Adv*. 2020;10:23108-23120.
94. Beaumont SK, Kyriakou G, Lambert RM. Identity of the Active Site in Gold Nanoparticle-Catalyzed Sonogashira Coupling of Phenylacetylene and Iodobenzene. *J Am Chem Soc*. 2010;132:12246-12248.
95. Goguet A, Ace M, Saih Y, Sa J, Kavanagh J, Hardacre C. Remarkable stability of ionic gold supported on sulfated lanthanum oxide. *Chem Commun*. 2009:4889-4891.
96. Kyriakou G, Beaumont SK, Humphrey SM, Antonetti C, Lambert RM. Sonogashira Coupling Catalyzed by Gold Nanoparticles: Does Homogeneous or Heterogeneous Catalysis Dominate? *ChemCatChem*. 2010;2:1444-1449.
97. Kanuru VK, Humphrey SM, Kyffin JMW, Jefferson DA, Burton JW, Armbruester M, Lambert RM. Evidence for heterogeneous Sonogashira coupling of phenylacetylene and iodobenzene catalyzed by well defined rhodium nanoparticles. *Dalton Trans*. 2009:7602-7605.
98. Boronat M, Combita D, Concepcion P, Corma A, Garcia H, Juarez R, Laursen S, de Dios Lopez-Castro J. Making C-C Bonds with Gold: Identification of Selective Gold Sites for Homo- and Cross-Coupling Reactions between Iodobenzene and Alkynes. *J Phys Chem C*. 2012;116:24855-24867.
99. Miyaura N, Yamada K, Suzuki A. A New Stereospecific Cross-coupling by the Palladium-catalyzed Reaction of 1-Alkenylboranes with 1-Alkenyl or 1-Alkynyl Halides. *Tetrahedron Lett*. 1979;20:3437-3440.
100. Miyaura N, Ishiyama T, Ishikawa M, Suzuki A. Palladium-catalyzed cross-coupling reactions of B-alkyl-9-BBN or trialkylboranes with aryl and 1-alkenyl halides. *Tetrahedron Lett*. 1986;27:6369-6372.
101. Corma A, Garcia H, Leyva A. Polyethylene Glycol as Scaffold and Solvent for Reusable C-C Coupling Homogeneous Pd Catalysts. *J Catal*. 2006;240:87-99.
102. Sanhes D, Raluy E, Rétory S, Saffon N, Teuma E, Gómez M. Unexpected activation of carbon–bromide bond promoted by palladium nanoparticles in Suzuki C–C couplings. *Dalton Trans*. 2010;39:9719-9726.
103. Lee AF, Ellis PJ, Fairlamb IJS, Wilson K. Surface catalysed Suzuki-Miyaura cross-coupling by Pd nanoparticles: an operando XAS study. *Dalton Trans*. 2010;39:10473-10482.
104. Narayanan R, El-Sayed MA. Effect of Catalysis on the Stability of Metallic Nanoparticles: Suzuki Reaction Catalyzed by PVP-Palladium Nanoparticles. *J Am Chem Soc*. 2003;125:8340-8347.
105. Narayanan R, El-Sayed MA. Catalysis with transition metal nanoparticles of different shapes. *Mater Res Soc Symp Proc*. 2006;900E:0900O1002.
106. Narayanan R, El-Sayed MA. Effect of Colloidal Catalysis on the Nanoparticle Size Distribution: Dendrimer-Pd vs PVP-Pd Nanoparticles Catalyzing the Suzuki Coupling Reaction. *J Phys Chem B*. 2004;108:8572-8580.
107. Kutubi SM, Sato K, Wada K, Yamamoto T, Matsumura S, Kusada K, Kobayashi H, Kitagawa H, Nagaoka K. Dual Lewis Acidic/Basic $Pd_{0.5}Ru_{0.5}$-Poly(*N*-vinyl-2-pyrrolidone) Alloyed Nanoparticle: Outstanding Catalytic Activity and Selectivity in Suzuki-Miyaura Cross-Coupling Reaction. *ChemCatChem*. 2015;7:3887-3894.
108. Yan X, Luo Y, Liu W, et al. Strategy used to synthesize high activity and low Pd catalyst for Suzuki coupling reaction: an experimental and theoretical investigation. *Phys Chem Chem Phys*. 2020;22:6222-6230.
109. Mora M, Jiménez-Sanchidrián C, Ruiz JR. Recent Advances in the Heterogeneous Palladium-Catalysed Suzuki Cross-Coupling Reaction. *Curr Org Chem*. 2012;16:1128-1150.
110. Paul S, Islam MM, Islam SM. Suzuki–Miyaura Reaction by Heterogeneously Supported Pd in Water: Recent Studies. *RSC Adv*. 2015;5:42193-42221.
111. Yang Y, Castano CE, Gupton BF, Reber AC, Khanna SN. A fundamental analysis of enhanced cross-coupling catalytic activity for palladium clusters on graphene supports. *Nanoscale*. 2016;8:19564-19572.

112. Li Y, Zhang Z, Shen J, Ye M. Hierarchical nanospheres based on Pd nanoparticles dispersed on carbon coated magnetite cores with a mesoporous ceria shell: a highly integrated multifunctional catalyst. *Dalton Trans*. 2015;44:16592-16601.
113. Guo L, Zhao X, Zhang R, Chen C, Chen J, Chen A, Liu X, Hou Z. Mesoporous spherical silica encapsulating Pd nanoparticles prepared by CO_2-induced mircoemulsion and catalytic application in Suzuki coupling reaction. *J Supercrit Fluids*. 2016;107:715-722.
114. Ubeda MA, Amoros P, Sanchez-Royo JF, El Haskouri J, Marcos MD, Perez-Pla F. Precatalyst or dosing-device? The $[Pd_2\{\mu\text{-}(C_6H_4)PPh_2\}_2\{\mu\text{-}O_2C(C_6H_5)\}_2]$ complex anchored on a carboxypolystyrene polymer as an effective supplier of palladium catalytically active nanoparticles for the Suzuki-Miyaura reaction. *J Catal*. 2020;381:26-37.
115. Hanif MA, Ebralidze II, Horton JH. Pd and S binding energies and Auger parameters on a model silica-supported Suzuki-Miyaura catalyst: Insights into catalyst activation. *Appl Surf Sci*. 2013;280:836-844.
116. Dutta P, Sarkar A. Palladium Nanoparticles Immobilized on Chemically Modified Silica Gel: Efficient Heterogeneous Catalyst for Suzuki, Stille and Sonogashira Cross-Coupling Reactions. *Adv Synth Catal*. 2011;353:2814-2822.
117. Dai C, Li X, Zhang A, Liu C, Song C, Guo X. Pd and Pd-CuO nanoparticles in hollow silicalite-1 single crystals for enhancing selectivity and activity for the Suzuki-Miyaura reaction. *RSC Adv*. 2015;5:40297-40302.
118. Fang M, Fan G, Li F. Highly Efficient Palladium Nanoparticles Homogeneously Immobilized on Microporous $ZnAl_2O_4$ Support for Suzuki-Miyaura Coupling Reaction. *Catal Lett*. 2014;144:142-150.
119. Yao Y, Patzig C, Hu Y, Scott RWJ. In Situ X-ray Absorption Spectroscopic Study of $Fe@Fe_xO_y/Pd$ and $Fe@Fe_xO_y/Cu$ Nanoparticle Catalysts Prepared by Galvanic Exchange Reactions. *J Phys Chem C*. 2015;119:21209-21218.
120. Niu J, Wang F, Zhu X, Zhao J, Ma J. One-pot synthesis of L-dopa-functionalized water-dispersible magnetite nano-palladium catalyst and its application in the Suzuki and Heck reactions in water: a novel and highly active catalyst. *RSC Adv*. 2014;4:37761-37766.
121. Keypour H, Saremi SG, Noroozi M, Veisi H. Synthesis of magnetically recyclable $Fe_3O_4@[(EtO)_3Si\text{-}L_1H]/Pd(II)$ nanocatalyst and application in Suzuki and Heck coupling reactions. *Appl Organomet Chem*. 2017;31:n/a.
122. Shan X, Sui N, Liu W, Liu M, Liu J. In situ generation of supported palladium nanoparticles from a Pd/Sn/S chalcogel and applications in 4-nitrophenol reduction and Suzuki coupling. *J Mater Chem A*. 2019;7:4446-4450.
123. Qiu J, Wang H, Zhao Y, Guan P, Li Z, Zhang H, Gao H, Zhang S, Wang J. Hierarchically porous covalent organic frameworks assembled in ionic liquids for highly effective catalysis of C-C coupling reactions. *Green Chem*. 2020;22:2605-2612.
124. Prakash SP, Gopidas KR. Palladium-Nanoparticle-Linked Organic Frameworks: Heterogeneous Recyclable Catalysts in Aqueous Medium. *ChemCatChem*. 2014;6:1641-1651.
125. Lu S, Hu Y, Wan S, McCaffrey R, Jin Y, Gu H, Zhang W. Synthesis of Ultrafine and Highly Dispersed Metal Nanoparticles Confined in a Thioether-Containing Covalent Organic Framework and Their Catalytic Applications. *J Am Chem Soc*. 2017;139:17082-17088.
126. You L-X, Yao S-X, Zhao B-B, Xiong G, Dragutan I, Dragutan V, liu x, Ding F, Sun Y. Striking dual functionality of the novel Pd@Eu-MOF nanocatalyst in $C(sp^2)$-$C(sp^2)$ bond-forming and CO_2 fixation reactions. *Dalton Trans*. 2020;49:6368-6376.
127. Mori K, Yamaguchi T, Ikurumi S, Yamashita H. Positive effects of the residual templates within the MCM-41 mesoporous silica channels in the metal-catalyzed reactions. *Chem Commun*. 2013;49:10468-10470.
128. Zhang M, Guan J, Zhang B, Su D, Williams CT, Liang C. Chemical Vapor Deposition of $Pd(C_3H_5)(C_5H_5)$ to Synthesize Pd@MOF-5 Catalysts for Suzuki Coupling Reaction. *Catal Lett*. 2012;142:313-318.

129. Dong W, Zhang L, Wang C, Feng C, Shang N, Gao S, Wang C. Palladium nanoparticles embedded in metal-organic framework derived porous carbon: synthesis and application for efficient Suzuki-Miyaura coupling reactions. *RSC Adv*. 2016;6:37118-37123.
130. Shang N, Gao S, Zhou X, Feng C, Wang Z, Wang C. Palladium nanoparticles encapsulated inside the pores of a metal-organic framework as a highly active catalyst for carbon-carbon cross-coupling. *RSC Adv*. 2014;4:54487-54493.
131. Panahi L, Naimi-Jamal MR, Mokhtari J. Ultrasound-assisted Suzuki-Miyaura reaction catalyzed by Pd@$Cu_2(NH_2\text{-}BDC)_2$(DABCO). *J Organomet Chem*. 2018;868:36-46.
132. Ding Y, Zhang L, Wu K-H, Feng Z, Shi W, Gao Q, Zhang B, Su DS. The influence of carbon surface chemistry on supported palladium nanoparticles in heterogeneous reactions. *J Colloid Interface Sci*. 2016;480:175-183.
133. Fareghi-Alamdari R, Haqiqi MG, Zekri N. Immobilized Pd(0) nanoparticles on phosphine-functionalized graphene as a highly active catalyst for Heck, Suzuki and N-arylation reactions. *New J Chem*. 2016;40:1287-1296.
134. Xiang G, He J, Li T, Zhuang J, Wang X. Rapid preparation of noble metal nanocrystals via facile coreduction with graphene oxide and their enhanced catalytic properties. *Nanoscale*. 2011;3:3737-3742.
135. Liu H, Zhang L, Wang N, Su DS. Palladium Nanoparticles Embedded in the Inner Surfaces of Carbon Nanotubes: Synthesis, Catalytic Activity, and Sinter Resistance. *Angew Chem, Int Ed*. 2014;53:12634-12638.
136. Shahbazi E, Bahrami K. Palladium Nanoparticles Doped on the Chitosan Nanofibers Modified with 2-Aminobenzaldehyde as a Nanocatalyst in Cross-Coupling Reactions. *ChemistrySelect*. 2020;5:5489-5496.
137. Manjare SB, Chaudhari RA, Thopate SR, Risbud KP, Badade SM. Resin loaded palladium nanoparticle catalyst, characterization and application in -C-C- coupling reaction. *SN Appl Sci*. 2020;2:988.
138. Wang K, Liu J, Zhang F, Zhang Q, Jiang H, Tong M, Xiao Y, Son Phan NT, Zhang F. Primary Amine-Functionalized Mesoporous Phenolic Resin-Supported Palladium Nanoparticles as an Effective and Stable Catalyst for Water-Medium Suzuki-Miyaura Coupling Reactions. *ACS Appl Mater Interfaces*. 2019;11:41238-41244.
139. Ul Islam R, Witcomb MJ, Scurrell MS, van Otterlo W, van der Lingen E, Mallick K. Metal-Polymer Hybrid Material as a Catalyst for the Heck Coupling Reaction Under Phosphine-Free Conditions. *Synth Commun*. 2011;41:3561-3572.
140. Chen Z, Liang Y, Jia D, Cui Z, Song W. Simple synthesis of sub-nanometer Pd clusters: high catalytic activity of Pd/PEG-PNIPAM in Suzuki reaction. *Chin J Catal*. 2017;38:651-657.
141. Zhang S, Shen X, Zheng Z, Ma Y, Qu Y. 3D graphene/nylon rope as a skeleton for noble metal nanocatalysts for highly efficient heterogeneous continuous-flow reactions. *J Mater Chem A*. 2015;3:10504-10511.
142. Alonso A, Macanas J, Shafir A, Munoz M, Vallribera A, Prodius D, Melnic S, Turta C, Muraviev DN. Donnan-exclusion-driven distribution of catalytic ferromagnetic nanoparticles synthesized in polymeric fibers. *Dalton Trans*. 2010;39:2579-2586.
143. Zheng Z, Li H, Liu T, Cao R. Monodisperse noble metal nanoparticles stabilized in SBA-15: Synthesis, characterization and application in microwave-assisted Suzuki-Miyaura coupling reaction. *J Catal*. 2010;270:268-274.
144. Esmaeilpour M, Javidi J, Dodeji FN, Hassannezhad H. Fe_3O_4@SiO_2-polymer-imid-Pd magnetic porous nanosphere as magnetically separable catalyst for Mizoroki-Heck and Suzuki-Miyaura coupling reactions. *J Iran Chem Soc*. 2014;11:1703-1715.
145. Guarnizo A, Angurell I, Rossell MD, Llorca J, Muller G, Seco M, Rossell O. 4-Mercaptophenyldiphenylphosphine as linker to immobilize Pd onto the surface of magnetite nanoparticles. Excellent catalytic efficiency of the system after partial linker removal. *RSC Adv*. 2015;5:91340-91348.

146. Wang F, Zhang Y, Du Z, Ren J, Qu X. Designed heterogeneous palladium catalysts for reversible light-controlled bioorthogonal catalysis in living cells. *Nat Commun*. 2018;9:1-8.
147. Oliveira RL, Kerstien J, Schomaecker R, Thomas A. Pd nanoparticles confined in mesoporous N-doped carbon silica supports: a synergistic effect between catalyst and support. *Catal Sci Technol*. 2020;10:1385-1394.
148. Adamo C, Amatore C, Ciofini I, Jutand A, Lakmini H. Mechanism of the Palladium-Catalyzed Homocoupling of Arylboronic Acids: Key Involvement of a Palladium Peroxo Complex. *J Am Chem Soc*. 2006;128:6829-6836.
149. Moreno-Mañas M, Pérez M, Pleixats R. Palladium-Catalyzed Suzuki-Type Self-Coupling of Arylboronic Acids. A Mechanistic Study. *J Org Chem*. 1996;61:2346-2351.
150. Thomas AA, Denmark SE. Pre-transmetalation Intermediates in the Suzuki-Miyaura Reaction Revealed: the Missing Link. *Science*. 2016;352:329-332.
151. Thomas AA, Zahrt AF, Delaney CP, Denmark SE. Elucidating the Role of the Boronic Esters in the Suzuki–Miyaura Reaction: Structural, Kinetic, and Computational Investigations. *J Am Chem Soc*. 2018;140:4401-4416.
152. Bhattacherjee D, Rahman M, Ghosh S, Bagdi AK, Zyryanov GV, Chupakhin ON, Das P, Hajra A. Advances in Transition-Metal Catalyzed Carbonylative Suzuki-Miyaura Coupling Reaction: An Update. *Adv Synth Catal*. 2021;363:1597-1624.
153. Sogutlu I, Mahmood EA, Ahmadizadeh Shendy S, Ebrahimiasl S, Vessally E. Recent progress in application of nanocatalysts for carbonylative Suzuki cross-coupling reactions. *RSC Adv*. 2021;11:2112-2125.
154. Zhu X, Niu J, Zhang F, Zhou J, Li X, Ma J. Preparation of recoverable Fe_3O_4@PANI-PdII core/shell catalysts for Suzuki carbonylative cross-coupling reactions. *New J Chem*. 2014;38:4622-4627.
155. Long Y, Liang K, Niu J, Tong X, Yuan B, Ma J. Agglomeration of Pd(0) nanoparticles causing different catalytic activities of Suzuki carbonylative cross-coupling reactions catalyzed by Pd(II) and Pd(0) immobilized on dopamine-functionalized magnetite nanoparticles. *New J Chem*. 2015;39:2988-2996.
156. Narayanan R, El-Sayed MA. Effect of Colloidal Nanocatalysis on the Metallic Nanoparticle Shape: The Suzuki Reaction. *Langmuir*. 2005;21:2027-2033.
157. Hu Y, Liu Y, Li Z, Sun Y. Highly Asymmetric, Interfaced Dimers Made of Au Nanoparticles and Bimetallic Nanoshells: Synthesis and Photoenhanced Catalysis. *Adv Funct Mater*. 2014;24:2828-2836.
158. Han D, Bao Z, Xing H, Yang Y, Ren Q, Zhang Z. Fabrication of plasmonic Au-Pd alloy nanoparticles for photocatalytic Suzuki-Miyaura reactions under ambient conditions. *Nanoscale*. 2017;9:6026-6032.
159. Pourjavadi PA, Keshavarzi N, Moghaddam FM, Hosseini SH. Magnetic Nanocomposite of Cross-Linked Melamine Groups Decorated with Large Amounts of Gold NPs: Reduction of Nitro Compounds and Suzuki-Miyaura Coupling Reactions in Aqueous Media. *ChemistrySelect*. 2018;3:2716-2722.
160. Sasmal S, Debnath M, Nandi SK, Haldar D. A urea-modified tryptophan based in situ reducing and stabilizing agent for the fabrication of gold nanoparticles as a Suzuki-Miyaura cross-coupling catalyst in water. *Nanoscale Adv*. 2019;1:1380-1386.
161. Akiyama T, Taniguchi T, Saito N, et al. Ligand-free Suzuki-Miyaura coupling using ruthenium(0) nanoparticles and a continuously irradiating microwave system. *Green Chem*. 2017;19:3357-3369.
162. Sahoo M, Mansingh S, Subudhi S, Mohapatra P, Parida K. A plasmonic AuPd bimetallic nanoalloy decorated over a GO/LDH hybrid nanocomposite via a green synthesis route for robust Suzuki coupling reactions: a paradigm shift towards a sustainable future. *Catal Sci Technol*. 2019;9:4678-4692.
163. Musza K, Szabados M, Adam AA, Konya Z, Kukovecz A, Sipos P, Palinko I. Mechanochemically modified hydrazine reduction method for the synthesis of nickel nanoparticles and their catalytic activities in the Suzuki-Miyaura cross-coupling reaction. *React Kinet, Mech Catal*. 2019;126:857-868.
164. Abdel-Fatah SM, Diaz-Sanchez M, Diaz-Garcia D, Prashar S, Abdel-Rahman LH, Gomez-Ruiz S. Nanostructured Metal Oxides Prepared from Schiff Base Metal Complexes: Study of the Catalytic

Activity in Selective Oxidation and C-C Coupling Reactions. *J Inorg Organomet Polym Mater*. 2020;30:1293-1305.
165. Sharma H, Sharma S, Sharma C, Paul S, Clark JH. Magnetically recoverable graphene oxide supported Co@Fe_3O_4/L-dopa for C-C cross-coupling and oxidation reactions in aqueous medium. *Mol Catal*. 2019;469:27-39.
166. Mohammadinezhad A, Akhlaghinia B. Fe_3O_4@Boehmite-NH_2-CoII NPs: an inexpensive and highly efficient heterogeneous magnetic nanocatalyst for the Suzuki-Miyaura and Heck-Mizoroki cross-coupling reactions. *Green Chem*. 2017;19:5625-5641.
167. Nasseri MA, Rezazadeh Z, Kazemnejadi M, Allahresani A. A Co-Cu bimetallic magnetic nanocatalyst with synergistic and bifunctional performance for the base-free Suzuki, Sonogashira, and C-N cross-coupling reactions in water. *Dalton Trans*. 2020;49:10645-10660.
168. Varun BV, Dhineshkumar J, Bettadapur KR, Siddaraju Y, Alagiri K, Prabhu KR. Recent advancements in dehydrogenative cross coupling reactions for C-C bond formation. *Tetrahedron Lett*. 2017;58:803-824.
169. Lakshman MK, Vuram PK. Cross-dehydrogenative coupling and oxidative-amination reactions of ethers and alcohols with aromatics and heteroaromatics. *Chem Sci*. 2017;8:5845-5888.
170. Wang J, Su P, Abdolmohammadi S, Vessally E. A walk around the application of nanocatalysts for cross-dehydrogenative coupling of C-H bonds. *RSC Adv*. 2019;9:41684-41702.
171. Tyagi A, Matsumoto T, Yamamoto A, Kato T, Yoshida H. Metal Cocatalyst Directing Photocatalytic Acetonylation of Toluene via Dehydrogenative Cross-Coupling with Acetone. *Catal Lett*. 2020;150:31-38.
172. Bai M, Xin H, Guo Z, Guo D, Wang Y, Zhao P, Li J. α-Alkylation of ketones with primary alcohols driven by visible light and bimetallic gold and palladium nanoparticles supported on transition metal oxide. *Appl Surf Sci*. 2017;391:617-626.
173. Alonso F, Arroyo A, Martin-Garcia I, Moglie Y. Cross-Dehydrogenative Coupling of Tertiary Amines and Terminal Alkynes Catalyzed by Copper Nanoparticles on Zeolite. *Adv Synth Catal*. 2015;357:3549-3561.
174. Martin-Garcia I, Alonso F. Synthesis of Dihydroindoloisoquinolines through Copper-Catalyzed Cross-Dehydrogenative Coupling of Tetrahydroisoquinolines and Nitroalkanes. *Chem Eur J*. 2018;24:18857-18862.
175. Qiang W, Liu X, Loh T-P. Supported Iridium Catalyst for the Green Synthesis of 3,3'-Bis(indolyl)methanes Using Methanol As the Bridging Methylene Source. *ACS Sustainable Chem Eng*. 2019;7:8429-8439.
176. Lin M, Dai L-X, Gu J, et al. Moderate oxidation levels of Ru nanoparticles enhance molecular oxygen activation for cross-dehydrogenative-coupling reactions via single electron transfer. *RSC Adv*. 2017;7:33078-33085.
177. Hili R, Yudin AK. Making carbon-nitrogen bonds in biological and chemical synthesis. *Nat Chem Biol*. 2006;2:284-287.
178. Insuasty D, Castillo J, Becerra D, Rojas H, Abonia R. Synthesis of biologically active molecules through multicomponent reactions. *Molecules*. 2020;25
179. Han YT, Jung J-W, Kim N-J. Recent Advances in the Synthesis of Biologically Active Cinnoline, Phthalazine and Quinoxaline Derivatives. *Curr Org Chem*. 2017;21:1265-1291.
180. Hartwig JF. Carbon-heteroatom bond formation catalyzed by organometallic complexes. *Nature*. 2008;455:314-322.
181. Achar TK, Bose A, Mal P. Mechanochemical synthesis of small organic molecules. *Beilstein J Org Chem*. 2017;13:1907-1931.
182. Kashin AS, Ananikov VP. Catalytic C-C and C-Heteroatom Bond Formation Reactions: In Situ Generated or Preformed Catalysts? Complicated Mechanistic Picture Behind Well-Known Experimental Procedures. *J Org Chem*. 2013;78:11117-11125.
183. Xu B, Haubrich J, Freyschlag CG, Madix RJ, Friend CM. Oxygen-assisted cross-coupling of methanol with alkyl alcohols on metallic gold. *Chem Sci*. 2010;1:310-314.

184. Xu B, Liu X, Haubrich J, Friend CM. Vapour-phase gold-surface-mediated coupling of aldehydes with methanol. *Nat Chem*. 2010;2:61-65.
185. Zugic B, Karakalos S, Stowers KJ, Biener MM, Biener J, Madix RJ, Friend CM. Continuous Catalytic Production of Methyl Acrylates from Unsaturated Alcohols by Gold: The Strong Effect of C=C Unsaturation on Reaction Selectivity. *ACS Catal*. 2016;6:1833-1839.
186. Han J, Gu F, Li Y. *N*-Doped Sub-3 nm Co Nanoparticles as Highly Efficient and Durable Aerobic Oxidative Coupling Catalysts. *Chem Asian J*. 2016;11:2594-2601.
187. Shimizu K-i, Kubo T, Satsuma A, Kamachi T, Yoshizawa K. Surface Oxygen Atom as a Cooperative Ligand in Pd Nanoparticle Catalysis for Selective Hydration of Nitriles to Amides in Water: Experimental and Theoretical Studies. *ACS Catal*. 2012;2:2467-2474.
188. Yang S, Wu C, Zhou H, Yang Y, Zhao Y, Wang C, Yang W, Xu J. An Ullmann C-O Coupling Reaction Catalyzed by Magnetic Copper Ferrite Nanoparticles. *Adv Synth Catal*. 2013;355:53-58.
189. Paul S, Pradhan K, Ghosh S, De SK, Das AR. Magnetically retrievable nanocrystalline nickel ferrite-catalyzed aerobic, ligand-free C-N, C-O and C-C cross-coupling reactions for the synthesis of a diversified library of heterocyclic molecules. *Adv Synth Catal*. 2014;356:1301-1316.
190. Moghaddam FM, Tavakoli G, Aliabadi A. Application of nickel ferrite and cobalt ferrite magnetic nanoparticles in C-O bond formation: a comparative study between their catalytic activities. *RSC Adv*. 2015;5:59142-59153.
191. Lu J, Behtash S, Heyden A. Theoretical Investigation of the Reaction Mechanism of the Decarboxylation and Decarbonylation of Propanoic Acid on Pd(111) Model Surfaces. *J Phys Chem C*. 2012;116:14328-14341.
192. Lu J, Faheem M, Behtash S, Heyden A. Theoretical investigation of the decarboxylation and decarbonylation mechanism of propanoic acid over a Ru(0001) model surface. *J Catal*. 2015;324:14-24.
193. Carabineiro SAC. Supported gold nanoparticles as catalysts for the oxidation of alcohols and alkanes. *Front Chem*. 2019;7:702.
194. Zhang Y, Zhang J, Zhang B, et al. Boosting the catalysis of gold by O_2 activation at Au-SiO_2 interface. *Nat Commun*. 2020;11:558.
195. Nguyen V-H, Nguyen B-S, Hu C, et al. Advances in designing Au nanoparticles for catalytic epoxidation of propylene with H_2 and O_2. *Catalysts*. 2020;10:442.
196. McEntee M, Tang W, Neurock M, Yates JT. Mechanistic Insights into the Catalytic Oxidation of Carboxylic Acids on Au/TiO_2: Partial Oxidation of Propionic and Butyric Acid to Gold Ketenylidene through Unsaturated Acids. *ACS Catal*. 2015;5:744-753.
197. So M-H, Liu Y, Ho C-M, Che C-M. Graphite-Supported Gold Nanoparticles as Efficient Catalyst for Aerobic Oxidation of Benzylic Amines to Imines and N-Substituted 1,2,3,4-Tetrahydroisoquinolines to Amides: Synthetic Applications and Mechanistic Study. *Chem Asian J*. 2009;4:1551-1561.
198. Yamaguchi K, Mizuno N. Efficient Heterogeneous Aerobic Oxidation of Amines by a Supported Ruthenium Catalyst. *Angew Chem Int Ed*. 2003;42:1480-1483.
199. Shi F, Tse MK, Zhou S, Pohl M-M, Radnik J, Huebner S, Jaehnisch K, Brueckner A, Beller M. Green and Efficient Synthesis of Sulfonamides Catalyzed by Nano-Ru/Fe_3O_4. *J Am Chem Soc*. 2009;131:1775-1779.
200. He J, Dhakshinamoorthy A, Primo A, Garcia H. Iron Nanoparticles Embedded in Graphitic Carbon Matrix as Heterogeneous Catalysts for the Oxidative C-N Coupling of Aromatic N-H Compounds and Amides. *ChemCatChem*. 2017;9:3003-3012.
201. Jesin I, Nandi GC. Recent Advances in the A^3 Coupling Reactions and their Applications. *Eur J Org Chem*. 2019;2019:2704-2720.
202. Peshkov VA, Pereshivko OP, Van der Eycken EV. A walk around the A^3-coupling. *Chem Soc Rev*. 2012;41:3790-3807.
203. Volkova Y, Baranin S, Zavarzin I. A^3 Coupling Reaction in the Synthesis of Heterocyclic Compounds. *Adv Synth Catal*. 2021;363:40-61.
204. Lauder K, Toscani A, Scalacci N, Castagnolo D. Synthesis and Reactivity of Propargylamines in Organic Chemistry. *Chem Rev*. 2017;117:14091-14200.

205. Nasrollahzadeh M, Sajjadi M, Ghorbannezhad F, Sajadi SM. A Review on Recent Advances in the Application of Nanocatalysts in A^3 Coupling Reactions. *Chem Rec*. 2018;18:1409-1473.
206. Saha TK, Das R. Progress in Synthesis of Propargylamine and Its Derivatives by Nanoparticle Catalysis via A^3 coupling: A Decade Update. *ChemistrySelect*. 2018;3:147-169.
207. Dang-Bao T, Pradel C, Favier I, Gómez M. Making Copper(0) Nanoparticles in Glycerol: A Straightforward Synthesis for a Multipurpose Catalyst. *Adv Synth Catal*. 2017;359:2832-2846.
208. Kang X, Chen S. Electronic conductivity of alkyne-capped ruthenium nanoparticles. *Nanoscale*. 2012;4:4183-4189.
209. Lin R, Amrute AP, Perez-Ramirez J. Halogen-Mediated Conversion of Hydrocarbons to Commodities. *Chem Rev*. 2017;117:4182-4247.
210. del Campo P, Martinez C, Corma A. Activation and conversion of alkanes in the confined space of zeolite-type materials. *Chem Soc Rev*. 2021;50:8511-8595.
211. Paunovic V, Zichittella G, Hemberger P, Bodi A, Perez-Ramirez J. Selective Methane Functionalization via Oxyhalogenation over Supported Noble Metal Nanoparticles. *ACS Catal*. 2019;9:1710-1725.
212. Jahangiri H, Bennett J, Mahjoubi P, Wilson K, Gu S. A review of advanced catalyst development for Fischer-Tropsch synthesis of hydrocarbons from biomass derived syn-gas. *Catal Sci Technol*. 2014;4:2210-2229.
213. Fischer N, Claeys M. In situ characterization of Fischer-Tropsch catalysts: a review. *J Phys D: Appl Phys*. 2020;53:293001.
214. Yang J, Ma W, Chen D, Holmen A, Davis BH. Fischer-Tropsch synthesis: A review of the effect of CO conversion on methane selectivity. *Appl Catal, A*. 2014;470:250-260.
215. Davis BH. Fischer-Tropsch Synthesis: Reaction mechanisms for iron catalysts. *Catal Today*. 2009;141:25-33.
216. Torres Galvis HM, Bitter JH, Davidian T, Ruitenbeek M, Dugulan AI, de Jong KP. Iron Particle Size Effects for Direct Production of Lower Olefins from Synthesis Gas. *J Am Chem Soc*. 2012;134:16207-16215.
217. Wezendonk TA, Sun X, Dugulan AI, van Hoof AJF, Hensen EJM, Kapteijn F, Gascon J. Controlled formation of iron carbides and their performance in Fischer-Tropsch synthesis. *J Catal*. 2018;362:106-117.
218. Bordet A, Lacroix L-M, Soulantica K, Chaudret B. A New Approach to the Mechanism of Fischer-Tropsch Synthesis Arising from Gas Phase NMR and Mass Spectrometry. *ChemCatChem*. 2016;8:1727-1731.
219. Ozbek MO, Niemantsverdriet JW. Methane, formaldehyde and methanol formation pathways from carbon monoxide and hydrogen on the (0 0 1) surface of the iron carbide χ-Fe_5C_2. *J Catal*. 2015;325:9-18.
220. Zhao Y, Zhao B, Liu J, et al. Oxide-Modified Nickel Photocatalyst for the Production of Hydrocarbons in Visible Light. *Angew Chem, Int Ed*. 2016;55:4215-4219.
221. Weststrate CJ, van Helden P, Niemantsverdriet JW. Reflections on the Fischer-Tropsch synthesis: Mechanistic issues from a surface science perspective. *Catal Today*. 2016;275:100-110.
222. Weststrate CJ, Sharma D, Garcia Rodriguez D, Gleeson MA, Fredriksson HOA, Niemantsverdriet JW. Mechanistic insight into carbon-carbon bond formation on cobalt under simulated Fischer-Tropsch synthesis conditions. *Nat Commun*. 2020;11:750.
223. Bertella F, Lopes CW, Foucher AC, Agostini G, Concepcion P, Stach EA, Martinez A. Insights into the Promotion with Ru of Co/TiO_2 Fischer-Tropsch Catalysts: An In Situ Spectroscopic Study. *ACS Catal*. 2020;10:6042-6057.
224. Chakraborty D, Nandi S, Mullangi D, Haldar S, Vinod CP, Vaidhyanathan R. Cu/Cu_2O Nanoparticles Supported on a Phenol-Pyridyl COF as a Heterogeneous Catalyst for the Synthesis of Unsymmetrical Diynes via Glaser-Hay Coupling. *ACS Appl Mater Interfaces*. 2019;11:15670-15679.